

ASD-TDR-62-1111

*AD A280 738*  
SUPERCONDUCTIVITY IN METALS AND ALLOYS

TECHNICAL DOCUMENTARY REPORT NO. ASD-TDR-62-1111

FEBRUARY 1963

DIRECTORATE OF MATERIALS AND PROCESSES  
AERONAUTICAL SYSTEMS DIVISION  
AIR FORCE SYSTEMS COMMAND  
WRIGHT-PATTERSON AIR FORCE BASE, OHIO

DTIC  
SELECTED  
JUN 10 1994  
S B D

PROJECT NO. 7371, TASK NO. 737102

PREPARED UNDER CONTRACT NO. AF33(657)7733

Prepared by

W. H. CHERRY	J. I. GITTLEMAN
G. D. CODY	J. J. HANAK
J. L. COOPER	M. RAYL
G. CULLEN	F. D. ROSI

DTIC QUALITY INSPECTED 2

DISTRIBUTION STATEMENT A  
Approved for public release  
Distribution Unlimited

RADIO CORPORATION OF AMERICA  
RCA LABORATORIES  
PRINCETON, NEW JERSEY

**Best  
Available  
Copy**

## FOREWORD

This report was prepared by RCA Laboratories under USAF Contract No. AF33(657)7733. The work was administered under the direction of the Directorate of Materials and Processes, Deputy for Technology, Aeronautical Systems Division.

This report covers work conducted from November 8, 1961 to November 7, 1962.

G. D. Cody and F. D. Rosi of RCA Laboratories were project engineer and project supervisor, respectively.

Accession For	
NTIS GRA&I	<input checked="" type="checkbox"/>
DTIC TAB	<input checked="" type="checkbox"/>
Unannounced	<input type="checkbox"/>
Justification	
By _____	
Distribution/ _____	
Availability Codes	
Dist	Avail and/or Special
A2	

## ABSTRACT

Measurements were made of the Kapitza resistance in tin and indium and its change at the superconducting transition. For comparison with theory, measurements were also made on the insulator, sapphire. An attempt to detect an electric field dependence of the Kapitza resistance in platinum had negative results.

A new method for the preparation of  $\beta$ -tungsten compound superconductors, such as  $Nb_3Sn$ , was developed. Both the properties of the deposited material and the extension of this method to such possible  $\beta$ -tungsten compounds as niobium germanide, niobium silicide, vanadium-gallium, vanadium silicide and niobium-gallium are described.

The transition temperature of niobium stannide is shown to depend not only on the stoichiometry, but also on the state of order of the lattice. Resistivity of  $Nb_3Sn$  is given as a function of temperature from 4.2°K to 370°K. Tunneling measurements on deposited  $Nb_3Sn$  indicate the existence of a bandgap ( $2\epsilon_0$ ). Preliminary results are compatible with the relation:  $2\epsilon_0 \approx 1.8 T_c$ .

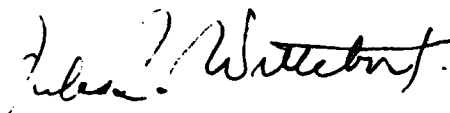
Penetration depth measurements were made on deposited  $Nb_3Sn$ . The temperature dependence is similar to that obtained for other superconductors, but the value of the penetration depth at  $T = 0^\circ K$  (2,880 Å) is almost an order of magnitude larger than that observed for soft superconductors. This value and the predictions of the BCS (Bardeen, Cooper, and Schrieffer, 1957) theory in the local limit are compared. A comparison is also made with recent theories of hard superconductors.

Quenching currents were measured on deposited  $Nb_3Sn$ . Preliminary results indicate a zero field quenching current close to that predicted by the Silsbee hypothesis assuming a thermodynamic critical field  $H_0 \approx 5,000$  gauss. For transverse fields the quenching current drops rapidly, whereas for longitudinal fields the quenching current rises. Comparison of these results are made with recent theories of hard superconductors.

Thermal conductivity measurements were made on  $Nb_3Sn$ . Preliminary results indicate qualitative agreement with the predictions of the microscopic theory of superconductivity.

In the Appendix, results are given from a study on the thermal effect of resistive current contacts on the quenching current of niobium stannide.

This Technical Documentary Report has been reviewed and is approved.



JULES I. WITTEBORT  
Chief, Thermophysics Branch  
Physics Laboratory  
Dir. of Materials & Processes

## TABLE OF CONTENTS

	<i>Page</i>
FOREWORD .....	iii
ABSTRACT .....	v
I. INTRODUCTION .....	1
II. KAPITZA RESISTANCE.....	3
A. Introduction .....	3
B. Experimental Procedure .....	4
C. Results and Discussion .....	6
D. The Electric Field Dependence of the Kapitza Resistance .....	8
III. VAPOR-DEPOSITION OF Nb <sub>3</sub> Sn .....	10
A. Introduction .....	10
B. Crystals and Films of Nb <sub>3</sub> Sn .....	10
C. Wires and Ribbons of Nb <sub>3</sub> Sn .....	11
D. The Deposition of Nb <sub>3</sub> Sn on Insulating Substrates .....	15
E. Physical Properties and Chemical Analysis .....	18
F. Critical Current Data .....	20
G. Nb <sub>3</sub> Sn Solenoid .....	22
IV. PROPERTIES OF Nb <sub>3</sub> Sn .....	24
A. Effect of Lattice Disorder on the Transition Temperature of Niobium Stannide ...	24
B. Resistivity of Deposited Nb <sub>3</sub> Sn .....	27
C. Tunneling in Superconducting Nb <sub>3</sub> Sn .....	29
D. Penetration Depth of Nb <sub>3</sub> Sn .....	31
E. Low Field Critical Currents in Nb <sub>3</sub> Sn .....	42
F. Thermal Conductivity of Nb <sub>3</sub> Sn .....	48
V. NEW MATERIALS .....	50
A. Vapor-Deposition of Niobium Germanide .....	50
B. Vapor-Deposition of Niobium Silicide .....	50
C. Vapor-Deposition of Vanadium-Gallium, Vanadium-Silicide and Niobium-Gallium .....	51
APPENDIX – Thermal Effect of Resistive Current Contacts on the Quenching Current of Niobium Stannide .....	52
A. Introduction .....	52
B. Results and Discussion .....	52
REFERENCES .....	58

## LIST OF ILLUSTRATIONS

<i>Figure</i>	<i>Page</i>
1. Schematic of thermal conductance cell .....	4
2. Typical resistance rise of thermometers vs. power into specimen heater .....	6
3. Kapitza resistance for superconducting tin .....	6
4. (a) Schematic arrangement in cryostat .....	8
(b) Schematic arrangement of detection system .....	9
5. Schematic diagram for vapor deposition of Nb <sub>3</sub> Sn .....	10
6. Polycrystalline vapor-deposited Nb <sub>3</sub> Sn .....	11
7. Schematic diagram for continuous vapor-deposition of niobium stannide wire or ribbon .....	12
8. (a) Vapor deposition of niobium stannide on tantalum wire (inner deposit is niobium stannide). Wire substrate diameter = 0.018 cm .....	14
(b) Niobium stannide on platinum wire. Wire substrate diameter = 0.018 cm .....	14
9. Niobium stannide vapor deposited on (a) nickel, (b) gold-plated nickel .....	15
10. Polished Nb <sub>3</sub> Sn on ceramic flats .....	16
11. Polished Nb <sub>3</sub> Sn deposit on a ceramic cylinder .....	16
12. Nb <sub>3</sub> Sn sample with current and potential leads .....	17
13. Nb <sub>3</sub> Sn deposit in a spiral groove of a ceramic flat .....	17
14. Critical current as a function of applied transverse field .....	20
15. Critical current density vs. transverse field for vapor-deposited niobium-tin with variable $T_c$ .....	21
16. Nb <sub>3</sub> Sn solenoid with cross-section of tape .....	22
17. Transition temperature vs. composition of $\beta$ -tungsten Nb-Sn .....	24
18. Lattice site occupancy-composition for ordered and disordered niobium-tin .....	25
19. Transition temperature vs. percent of tin sites occupied by niobium for $\beta$ -tungsten Nb-Sn .....	26
20. Resistivity of Nb <sub>3</sub> Sn .....	28
21. I-V characteristics of Nb <sub>3</sub> Sn tunnel diodes .....	29
22. Relative density of states Nb <sub>3</sub> Sn .....	31
23. Cross-section of deposited Nb <sub>3</sub> Sn sample 43-4, magnified 400X. Sample nickel plated and polished, but not etched .....	32
24. Cross-section Nb <sub>3</sub> Sn sample 43-4 (2304X magnification) .....	32
25. Schematic of penetration depth apparatus .....	33
26. Anderson inductance bridge .....	34
27. Inductance change with respect to 4.22°K vs. T .....	35

## LIST OF ILLUSTRATIONS (Continued)

<i>Figure</i>	<i>Page</i>
28. AC resistance vs. T .....	36
29. Inductance change vs. Y for Nb <sub>3</sub> Sn .....	38
30. Inductance change vs. Y for lead .....	39
31. Quenching current vs. field at constant angle .....	43
32. Quenching current vs. angle at constant field .....	45
33. Possible quenching curves (schematic) .....	46
34. Temperature variation of thermal conductivity in Nb <sub>3</sub> Sn #53 .....	49
35. $K_s/K_n$ vs. $T/T_c$ for Nb <sub>3</sub> Sn #53 .....	49
36. Circuit diagram for quenching current measurements .....	53
37. Variation of quenching current with contact area .....	54
38. Contact resistance and power dissipation vs. reciprocal contact area .....	54
39. Contact power dissipation vs. quenching current .....	55
40. Contact power dissipation vs. quenching current .....	56

## LIST OF TABLES

<i>Table</i>	<i>Page</i>
I. Kapitza Resistance of Tin, Indium, Lead, and Sapphire .....	7
II. Some Physical Properties of Vapor-Deposited Niobium Stannide .....	18
III. Mass Spectrograph (MS 7) Analytical Results for Vapor-Deposited Niobium Stannide Ribbon .....	19
IV. Performance of Nb <sub>3</sub> Sn Solenoid .....	23
V. Lattice Disorder and $T_c$ of Unannealed and Annealed Vapor-Deposited Niobium Stannide, Nb <sub>4.1</sub> Sn .....	27
VI. Dimensions and Field Data for Nb <sub>3</sub> Sn #40 .....	44

## I. INTRODUCTION

The object of this contract has been: 1) to study the structure sensitive factors affecting the kinetics of the transition between the normal and superconducting states of selected metals, metal alloys, and intermetallic compounds, and 2) to explore the area of intermetallic compounds and compound alloys for new superconductors. This report\* is intended to give a summary of work done under this Contract during the period November 8, 1961 to November 7, 1962. For completeness, some RCA-supported research on superconductivity has been included where the results are relevant to the objectives of the contract. Although the present report is self-contained, reference to previous Contract Reports (RCA 1961) will be helpful in understanding the motivation and development of the present research program.

Section II of this report is concerned with the thermal contact resistance between solids and liquid helium II; i.e., the Kapitza resistance. This boundary resistance is important for the kinetics of the superconducting to normal transition (Cherry and Gittleman 1960) but is also of importance in understanding the coupling between energy transfer in superconductors and energy transfer in superfluid liquid helium. Measurements are presented on the change in the Kapitza resistance of tin and indium at the superconducting transition. Whereas in lead the Kapitza resistance changes by a factor of two (Challis, 1960), in tin and indium the change is less than 10%. Comparison is made of these results with current theories of the Kapitza resistance (Little, 1961) and the BCS theory of superconductivity (Bardeen, Cooper, and Schrieffer, 1957). An attempt was made to determine whether tunneling of the electrons into the superfluid helium was significant for the size of the Kapitza resistance, but with negative results.

Section III of this report concerns the preparation of single-phase  $Nb_3Sn$ . This material has the highest transition temperature of any known superconductor ( $18^\circ K$ ) and appears to support superconductivity to fields at least of the order of 170,000 gauss. Up to the present work,  $Nb_3Sn$  has been prepared either by sintering or arc-melting, and the resultant material was both porous and multiphase. The present technique involves the deposition of  $Nb_3Sn$  from the mixed chlorides, and has produced deposits of crystalline  $Nb_3Sn$  on both metals and insulators. A discussion is given of the method, and the properties of the deposited material. The importance of this technique for any understanding of  $Nb_3Sn$  is apparent. Only with well-defined material can one expect the fruitful collaboration of theory and experiment which was so successful for soft superconductors. The method has also proved of practical importance for the construction of high field superconducting solenoids. As an example, a 10-K gauss, 2-in. inner diameter solenoid is described, which was wound with 500 meters of  $Nb_3Sn$  deposited ribbon.

Section IV of this report covers research done on  $Nb_3Sn$  since the discovery of the vapor deposition process. This part of the research program had two purposes: (1) to characterize the superconducting state of  $Nb_3Sn$  as completely as possible and through this characterization determine the validity of present theories of superconductivity, and (2) to use the understanding of the behavior of  $Nb_3Sn$  to obtain superconductors of higher transition temperature and satisfactory magnetic and mechanical properties in forms suitable for research and application.

---

\* Manuscript released by the authors 2 January 1963 for publication as an ASD Technical Documentary Report.



One important topic in this section concerns the relation of the state of order of the  $Nb_3Sn$  lattice to the transition temperature. It has been shown in the past year that the stoichiometry of niobium stannide is not sufficient to determine the transition, but the ordering of the atoms on the sublattices must be specified as well. Although this effect was discovered at RCA on the basis of deposited material, it was also obtained for sintered material (Reed, Gatos, LaFleur, and Roddy, 1962). It has great importance for any materials work, since generalizations based only on stoichiometry may be somewhat questionable in systems with a broad range of stoichiometry as in niobium stannide. The theoretical significance of this result is difficult to determine in the light of the present simplified theory.

Other properties of  $Nb_3Sn$  that have been examined for the first time include the superconducting penetration depth, the bandgap (through tunneling), the thermal conductivity in the superconducting state, and indeed, such a "prosaic" quantity as the electrical resistivity and its temperature dependence. It is hoped to acquire sufficient information on  $Nb_3Sn$  as to make serious theoretical work worthwhile. Although much of the work described is preliminary, it appears now that the BCS theory applies qualitatively even to such an extreme superconductor as  $Nb_3Sn$ . The only modification required is in the direction of introducing "local" rather than "non-local" electrodynamics, (e.g., Gor'kov, 1960, Parmenter 1962). An important conclusion of this section of the report is that  $Nb_3Sn$  has a penetration depth considerably larger than its mean free path. Such a condition can be shown to lead to the persistence of superconductivity to extremely high magnetic fields and, hence, may be responsible for the high-field, high-current superconductivity displayed by  $Nb_3Sn$ .

Section V of this report is concerned with materials preparation. The success of the gas phase deposition process for  $Nb_3Sn$  showed that it might be possible to prepare other high-transition-temperature  $\beta$ -tungsten materials in this same manner. Indeed, it was thought possible to obtain materials that had not yet been synthesized due to difficulties in preparation. This section reports on the preparation of  $Nb_3Ge$ ,  $Nb_3Si$ ,  $V_3Si$ , and  $Nb_3Ga$ , as well as on the attempts at the preparation of  $V_3Ga$ . Preliminary results indicate that, although there are problems, the gas phase deposition method is a convenient and fruitful one for the preparation of these compounds in single-phase, high-density form.

The Appendix of this report is a technical discussion on some of the problems connected with the evaluation of the high-field-current properties of hard superconductors, such as  $Nb_3Sn$ .

## II. KAPITZA RESISTANCE

### A. INTRODUCTION

The existence of a thermal contact resistance between a solid body and liquid helium was first observed in 1941 by Kapitza, and this phenomenon has since been known as the Kapitza resistance. Khalatnikov (1952) showed that indeed a temperature jump was to be expected at the interface between the solid and liquid helium under the conditions of heat flow between the two media because of the acoustic mismatch at the boundary. His calculations predicted values of Kapitza resistance which varied as  $T^{-3}$ , but were several orders of magnitude larger than the experimental values available at the time.

Little (1959) analyzed, in detail, the conduction of heat across the interface between two dissimilar solids via phonon transport. Again, because of the mismatch of acoustical properties, he calculated the heat transport to be proportional to  $T^3\Delta T$  in the limit of small heat flow, where  $\Delta T$  is the temperature discontinuity at the interface between the two media. Whereas Little's calculations seemed to compare favorably with the observations of heat transfer between dissimilar solids, particularly between metals and paramagnetic salts, the theory, when applied to a metal-liquid helium interface, led to anomalously high values of Kapitza resistance. This, perhaps, was to be expected in view of Khalatnikov's calculations. The reason for the high calculated value of Kapitza resistance is clear. Because of the very large acoustical mismatch between liquid helium and a metal, only those phonons of the liquid which impinge on the metal surface and whose velocities are confined to a very narrow cone about the normal to the interface can be refracted into the metal, all the remaining phonons being totally reflected. The resulting inefficient transfer of phonons across the interface gives rise to a very large temperature discontinuity in order to maintain a given heat flow.

Little speculated that, in the case of a metal-liquid helium interface, the totally reflected phonons of the liquid were coupled to the conduction electrons of the metal thereby providing a mechanism for heat transport which acted in parallel with that derived from the Khalatnikov-Little theory. This could substantially lower the net Kapitza resistance. Recently, Little (1961) calculated the heat transport across the interface based on the above model. The "totally reflected" phonons produce a periodic disturbance of the metal lattice which decays exponentially with distance from the interface. The resulting displacement of the lattice ions in the neighborhood of the interface then provides the interaction which couples the conduction electrons with the "totally reflected" phonons. Little estimates, from his calculations, a Kapitza resistance of the order of  $\frac{10^3}{T^3} \frac{\text{°K-cm}^2}{\text{watt}}$ . Although this is somewhat less than that computed from the simple phonon transport theory, it is still about two orders of magnitude larger than the experimentally reported values.

Little (1959, 1961) pointed out that if this mechanism is an important one, there should be a difference between the values of the Kapitza resistance of a superconductor in its superconducting state and in its normal state. In Little's theory, for superconductors, it is only the quasi-particle which can interact with the surface phonons; and since the number of such particles which are thermally excited decrease roughly as  $\exp(-\frac{3.5T_c}{T})$  and the number of surface phonons capable

of creating such particles decrease in like manner, at sufficiently small  $T/T_c$  the Kapitza resistance for a metal in the superconducting state should be larger than when the metal is in its normal state.

To check the importance of this mechanism, measurements have been made of the Kapitza resistance of superconducting and normal tin and indium specimens, and a crystalline sapphire for which Little's mechanism should not apply because of the absence of conductor electrons. Observations have also been made on the effect of electric fields on the Kapitza resistance of platinum. The discussion of this latter effect will be delayed until later. Preliminary results for tin and indium have been reported earlier (RCA, 1961), and the more complete work will be described here along with a comparison to similar work reported elsewhere.

## B. EXPERIMENTAL PROCEDURE

The measurements on all specimens were made in a cell of the type shown in Fig. 1. All the thermometers were 1/10-watt, 220-ohm Allen-Bradley resistors with the outer casings replaced by thin copper sleeves insulated from the resistors by a thin layer of GE7031 adhesive

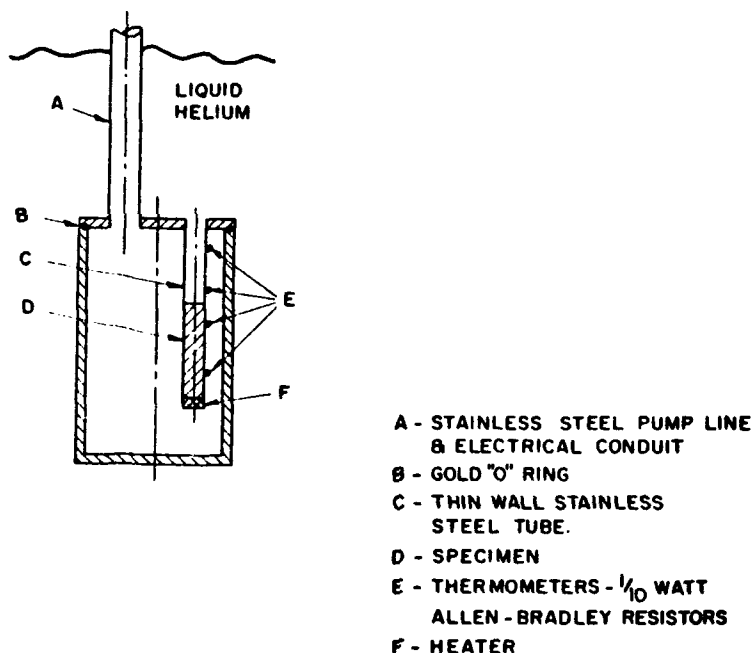


Fig. 1. Schematic of thermal conductance cell.

in a manner suggested by P. Lindenfeld (1961). For the metal specimens, the thermometers were soldered directly to the metal; for the sapphire specimen, the thermometers were attached using the GE7031 adhesive. The thermometer resistances were measured on a 20-cps Wheatstone bridge.

The specimens were in the form of rods about 0.2 in. in diameter and about 1.75 in. long which were sealed into a stainless steel tube having a wall thickness of .005 in. which formed

the supporting wall for the column of liquid helium that was in contact with the specimen end surface. The metal specimens were soldered directly to the tube, whereas the sapphire was sealed to the tube with an epoxy resin. The ends of the specimens in contact with the bath were machine-polished in the case of the metals, and hand-polished in the case of the sapphire.

The thermometers were calibrated against the vapor pressure of the liquid helium bath with helium exchange gas in the cell and under high vacuum conditions in the temperature range of 1.3°K to 2.0°K to insure that the thermometers achieved thermal equilibrium with the latter via contact with the specimens only. Since all measurements were made below the  $\lambda$ -point of liquid helium, the thermometers mounted on the stainless steel tube indicated the bath temperature for all heat levels used in the experiments.

The Kapitza resistance was measured in the following way. A dc heat current was made to flow along the specimen into the helium column by means of a heater cemented to the vacuum end of the specimen, as shown in Fig. 1. The temperature rise of each of the thermometers mounted on the specimen was measured as a function of the heat input. The temperature rise per unit heat flow on the solid side of the helium-solid interface was determined by extrapolating the temperature gradient along the rod to the interface. Although, with the exception of superconducting lead, for the present specimens the temperature rise of the thermometer located nearest to the interface did not differ from that at the interface by an experimentally significant amount. The temperature on the liquid side of the interface was taken to be the same as the bath temperature. The Kapitza resistance was then calculated from:

$$R_k = \frac{\Delta T_k}{q} a,$$

where

$$R_k = \text{the Kapitza resistance,}$$

$$\frac{\Delta T_k}{q} = \text{the temperature discontinuity at the interface per unit heat flow}$$

$$a = \text{the interface cross-sectional area.}$$

In the case of the metal specimens, data were taken over the entire temperature range when the specimens were superconducting. Then the entire procedure was repeated when the specimens were made normal with a magnetic field. This procedure was adopted, rather than switching the specimen between its superconducting and normal phases at a given temperature to avoid the trapping of normal regions in the vicinity of the interface and thus introducing unnecessary errors and scatter. The magnetoresistance of the thermometers was checked at magnetic fields greater than the critical value, and was found to be small enough to be experimentally insignificant.

The effect of magnetic field on the Kapitza resistance of (normal) lead has already been shown to be quite small by Challis (1960). A similar study has not been made for either tin or indium.

Temperature rise data were taken for heat inputs up to about 5 mw, since for higher heat fluxes the nonlinear relationship between resistance and temperature of the resistance thermometers

made the determination of the temperature rise awkward. Figure 2 is typical of the resistance rise vs. heat flux data obtained in the present experiments. The dashed portion is the expected deviation from linearity due to the nonlinearity of the resistance thermometers. For the data shown the heater resistance was 760 ohms.

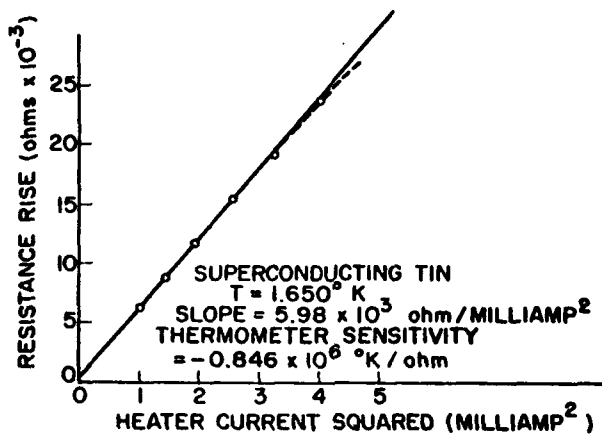


Fig. 2. Typical resistance rise of thermometers vs. power into specimen heater.

### C. RESULTS AND DISCUSSION

Figure 3 is typical of the Kapitza resistance vs. temperature data for all the specimens in both form and scatter. The circles represent the present experimental points. The curve was determined by assuming that the Kapitza resistance had the form  $R_k = A/T^3$ , and computing  $A$  for

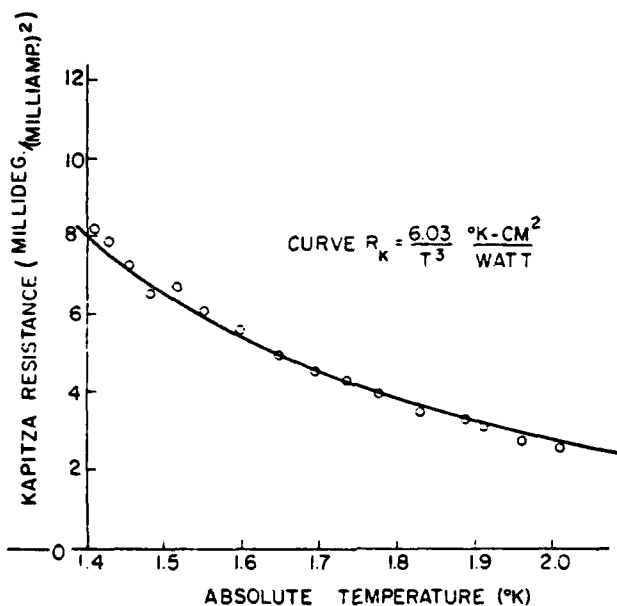


Fig. 3. Kapitza resistance for superconducting tin.

each experimental point, the average value of  $A$  for all the data was then used to plot the curve. In like manner  $T^{-2}$  and  $T^{-4}$  relations were attempted but each failed to fit the data over the whole of the temperature range. No claim is made that a noninteger exponent near 3 would not produce a better fit to the data; no effort was made to determine it. Table I is a summary of all of the present results. Included in the table for comparison are the results for lead as reported by Challis (1960).

TABLE I  
KAPITZA RESISTANCE OF TIN, INDIUM, LEAD, AND SAPPHIRE

SUBSTANCE	NORMAL STATE KAPITZA RESISTANCE ( $^{\circ}\text{K}\cdot\text{cm}^2/\text{watt}$ )	SUPERCONDUCTING STATE KAPITZA RESISTANCE ( $^{\circ}\text{K}\cdot\text{cm}^2/\text{watt}$ )	% DIFF.	$T_c$ ( $^{\circ}\text{K}$ )	ROOM TEMPERATURE RESISTIVITY OHM ( $\Omega\cdot\text{cm} \times 10^6$ )
Tin	$5.48/T^3$	$6.03/T^3$	10.6	3.74	11.5
Indium	$9.54/T^3$	$10.1/T^3$	5.9	3.37	8.4
Lead	$7/T^3$	<i>Faster than <math>T^3</math></i>	200-300	7.2	22
Sapphire	$44.1/T^3$	---	---	--	--

To ensure that the large differences in the normal and superconducting Kapitza resistance values of lead as reported by Challis (1960) and the small differences observed for tin and indium were not due to experimental discrepancy, the Kapitza resistance of lead was measured at several temperatures. Essential agreement with Challis' results were obtained. Qualitatively, at least, an explanation for the difference between lead and tin or indium can be found in Little's theory (Little, 1961). First, since lead has a larger superconducting energy gap (approximately  $3.5 kT_c$ ) than either tin or indium, in the experimental temperature range there are fewer quasi-particles to interact with the surface phonons as well as fewer surface phonons which are energetic enough to excite quasi-particles from the superconducting ground state. Thus, the superconducting Kapitza resistance should be larger for lead. Second, since the coupling between the electrons and the surface phonons is proportional to the phonon-electron interaction, which is larger in lead than in either tin or indium as evidenced by its higher critical temperature and larger room temperature resistivity, the Kapitza resistance for lead should be less than for the other metals.

Unfortunately, the reported value of the Kapitza resistance for normal lead is not less than for normal tin, but is larger by about 15%. However, this may be due to experimental uncertainties in determining the absolute value of the Kapitza resistance, such as the uncertainty of knowing the total effective area in contact with the helium. A more serious discrepancy with theory is the fact that, well below the critical temperature, the superconducting Kapitza resistance is expected to vary as  $\exp\left(\frac{3.5T_c}{T}\right)$  rather than as  $T^{-3}$  which is predicted for normal metals. This has never been observed, although Challis (1960) does report departures from the  $T^{-3}$  law for superconducting lead.

As can be seen from Table I, the Kapitza resistance of the normal metals appears to be about two orders of magnitude smaller than that predicted by Little's theory (Little, 1961). The Kapitza

resistance was measured for a single crystal sapphire rod which has essentially no conduction electrons and, therefore, should behave according to the older Khalatnikov-Little theory (Khalatnikov, 1952, Little, 1959). Although, as is shown in Table 1, the Kapitza resistance of the sapphire was appreciably higher than for the normal metals, its value falls far short of the nearly

$\frac{10^4}{T^3} \frac{^\circ K \cdot cm^2}{watt}$  value expected from the theory.

There exists, then, a strong suggestion that there are other important processes, acting in parallel with the one proposed by Little, for transporting heat energy across an interface. The mechanisms for these processes, if they exist, have thus far eluded discovery. It is, perhaps, appropriate to mention a possible shorting mechanism which was present in our experiment. In sealing the specimens into the stainless steel tube a lap type joint was made so that a fraction of the heat flux was able to bypass the solid-liquid interface via the stainless steel. However, a simple calculation showed that even in the case of sapphire, which exhibited the highest measured Kapitza resistance, the diverted heat flux should amount to not more than a percent or two of the total.

#### D. THE ELECTRIC FIELD DEPENDENCE OF KAPITZA RESISTANCE

At the 1961 spring meeting of the American Physical Society (Washington, D.C., April 24-27, 1961) in a post-paper discussion, Professor F. Bloch suggested a possible new mechanism for the transport of heat across a liquid-metal interface. It was, in a sense, the inverse of the mechanism proposed by Little (1961) in that it involved a coupling between the phonon wave functions of the liquid and that part of the electronic wave functions of the metal which "leaked" into the helium bath.

To test for the existence of this mechanism and, at the same time, to separate it from other possible mechanisms the following experiment was set up. In the apparatus shown in Fig. 1, a platinum rod was mounted in the manner described earlier for a Kapitza resistance measurement. Platinum was chosen because of its relatively high resistance to surface corrosion and because of its high thermal diffusivity at low temperatures. A high-voltage probe was located in the helium column in close proximity to the platinum surface, and was designed to give a minimum field gradient to the stainless steel supporting tube. The arrangement is shown schematically in Fig. 4a.

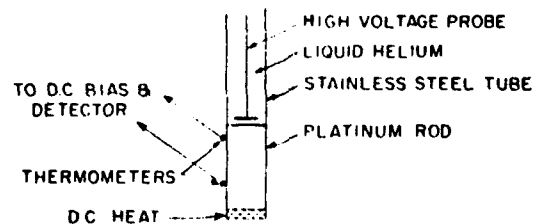


Fig. 4a. Schematic arrangement in cryostat.

With a dc heat flux flowing through the platinum rod to the helium bath, it was hoped that an ac electric field would periodically vary the distance the electronic wave functions "leaked" into the helium and thus modulate the coupling between these wave functions and the phonons.

The resulting modulation of the Kapitza resistance could then be observed as an ac temperature variation at one of the thermometers attached to the platinum, in a manner as indicated in Fig. 4b.

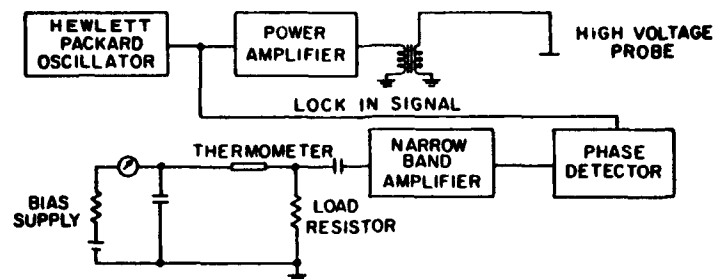


Fig. 4b. Schematic arrangement of detection system.

The maximum electric field available was about 100,000 volts/cm peak to peak. The electric field was calculated from the measured voltage applied to the probe and the measured spacing between the probe and the platinum surface. The spacing was also estimated by assuming that the probe and platinum surface formed a parallel plate condenser, and calculating its capacity by measuring the displacement current observed at the frequencies used. The spacing was about 0.3 mm. The output of the phase detector was observed both with the heat current on and off, and with the electric field on and off. With the above field values and with dc heat currents up to about 5 mw, no significant signal was observed at frequencies of 500 cps and 150 cps. From the sensitivity of our detection apparatus one must conclude that, in the temperature range of 1.4°K to 1.8°K, the ratio of the ac part of the Kapitza resistance to the total Kapitza resistance was less than about 1 part in  $10^7$ .

Since the size of the effect proposed by Bloch has not been estimated, one cannot evaluate these negative results in relation to the proposed mechanism. It is possible, for example, that in the light of a complete theory of the mechanism the high work function of platinum may preclude observation of the mechanism at the applied electric fields.



### III. VAPOR-DEPOSITION OF $Nb_3Sn$

#### A. INTRODUCTION

The vapor-phase technique for the deposition of niobium stannide has been developed at RCA (1961) and described in detail under a previous contract. In the past year, this work has been essentially concluded; and the progress that has been made in perfecting, understanding, and utilizing the process is included in a detailed description of the process.

#### B. CRYSTALS AND FILMS OF $Nb_3Sn$

Preparation of  $Nb_3Sn$  by gas-phase reactions appeared to be feasible because both niobium and tin metals can be obtained by reduction of their respective gaseous chlorides by hydrogen at temperatures well below  $1000^\circ C$ , as described by Sibert et al (1958) and Gonser and Slowter (1938). Hence, a simultaneous reduction of a mixture of these chlorides could be reasonably expected to yield  $Nb_3Sn$  directly without the intermediate formation of the free metals.

In initial attempts, two different pairs of chlorides  $NbCl_5-SnCl_2$  and  $NbCl_5-SnCl_4$  were used as starting materials. The apparatus had three temperature zones and an open end for a dynamic-flow operation. In each case  $Nb_3Sn$  film deposits were formed with crystal structure and  $T_c$  identical to the sintered compound. However, in these attempts difficulties were encountered in handling hygroscopic chlorides and in adjusting their partial pressures to appropriate values. The solution to these problems was found in the construction of an apparatus where sintered  $Nb_3Sn$  is used as the starting material, which is then directly chlorinated with chlorine gas, and where the resulting mixture of gaseous metal chlorides (mainly  $NbCl_5$  and  $SnCl_2$ ) is converted back to  $Nb_3Sn$  simply by introducing hydrogen. This apparatus is schematically shown in detail in Fig. 5. It should be

- |  |  |
|--|--|
| A = KANTHAL RESISTANCE FURNACE                   | F = POWDERED, SINTERED $Nb_3Sn$  |
| B = REACTION TUBE, QUARTZ, L-120cm,<br>I.D. 26mm | G = EXHAUST GASES  |
| C = QUARTZ CHLORINATION TUBE,<br>I.D. 10mm       | H = GAS-PHASE DEPOSITED $Nb_3Sn$<br>CRYSTALS                               |
| D = CHLORINE INLET                               | I = GAS-PHASE DEPOSITED $Nb_3Sn$ FILMS<br>INSIDE 8cm QUARTZ TUBE 15mm I.D. |
| E = HYDROGEN INLET                               | J = $Nb_3Sn$ FILMS CONTAINING BLACK<br>IMPURITIES                          |

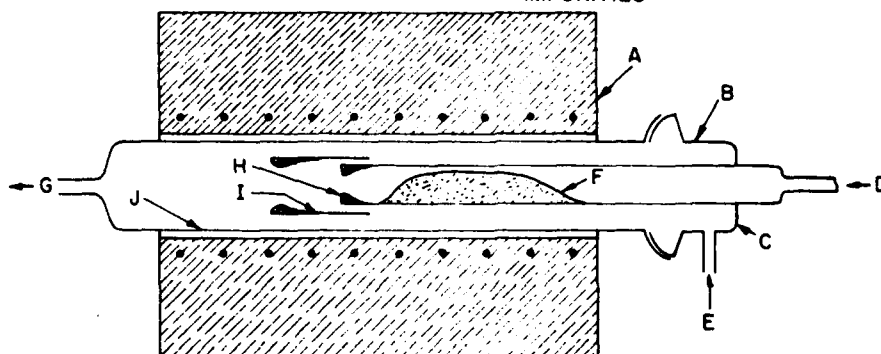


Fig. 5. Schematic diagram for vapor deposition of  $Nb_3Sn$ .

pointed out that although the chlorination and the reduction are carried out at the same temperature, at the chlorination site the temperature is always visibly higher due to the highly exothermic reactions taking place. The rate of flow of the chlorides and to some extent the rate of deposition of  $Nb_3Sn$  are controlled by regulating the rate of flow of chlorine gas. The temperature of the furnace can be maintained in the range of 900-1200°C with good results, although formation of  $Nb_3Sn$  was observed as low as 730°C. It was not possible to go to temperatures much above 1200°C because of the deterioration of the quartz apparatus. The deposition was usually allowed to run from one to three hours during which time up to 15g of sintered  $Nb_3Sn$  was consumed and about 25 to 75 percent of this amount redeposited as  $Nb_3Sn$ . The remainder was deposited as other species, usually a black cubic impurity with  $a = 5.94 \text{ \AA}$ , or passed out of the exhaust as unreacted chlorides.  $Nb_3Sn$  deposited in the form of single-phase polycrystals at *H* (Fig. 5) and as polycrystalline films in tube I; outside of these areas, at *J*, films containing  $Nb_3Sn$  also formed, but they always contained other codeposited species in amounts increasing with the distance away from tube I. These observations indicate that an increase in the ratio of HCl to the metal chlorides is detrimental to the deposition of  $Nb_3Sn$ . Examples of vapor-deposited  $Nb_3Sn$  are shown in Fig. 6.

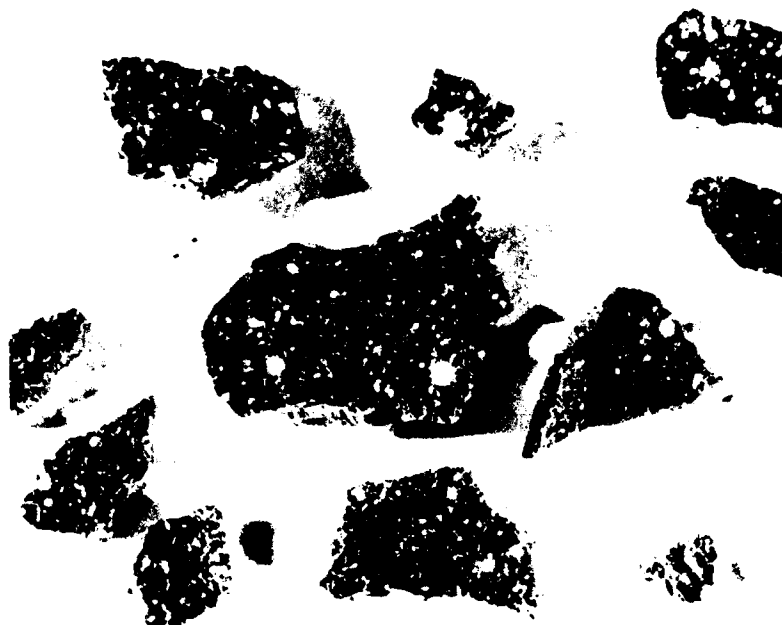


Fig. 6. Polycrystalline vapor-deposited  $Nb_3Sn$ .

### C. WIRES AND RIBBONS OF $Nb_3Sn$

The vapor-deposition process of  $Nb_3Sn$  was soon recognized to be well suited for coating of refractory metal wires and ribbons for superconducting solenoid applications; however, the process had to be made continuous to be capable of producing great lengths of  $Nb_3Sn$  in this form. This requirement implied that during the process the walls of the apparatus had to be kept free from deposition of  $Nb_3Sn$  or other condensations which would tend to congest the apparatus.

Experience gained with the deposition of  $Nb_3Sn$  crystals indicated that the approach to this problem was to maintain the apparatus at a temperature which would be too low for  $Nb_3Sn$  to form, but high enough to volatilize the metal chlorides. The deposition of  $Nb_3Sn$  on the wire surface would then be accomplished by pulling the wire through the apparatus, and heating it by its own resistance to a temperature necessary for the process to occur.

A schematic diagram of such apparatus appears in Fig. 7. The apparatus is constructed of quartz, and consists of two parts: One is the vertical part, or "the vertical chlorination chamber," where sintered niobium-tin ingot burns in chlorine gas, forming volatile chlorides, and moves downward as it is consumed. Additional ingots are introduced through a lock chamber on top (not shown) to ensure the continuity of the process. The second, the horizontal part, is the deposition chamber designed for a dynamic flow operation. The ends of the chamber are fitted with slotted graphite rods which serve as partial gas plugs and also as sliding electrical contacts for heating to the desired temperature the ribbon being deposited with  $Nb_3Sn$ . A variable-speed electric motor pulls the deposited wire or ribbon through the deposition chamber.

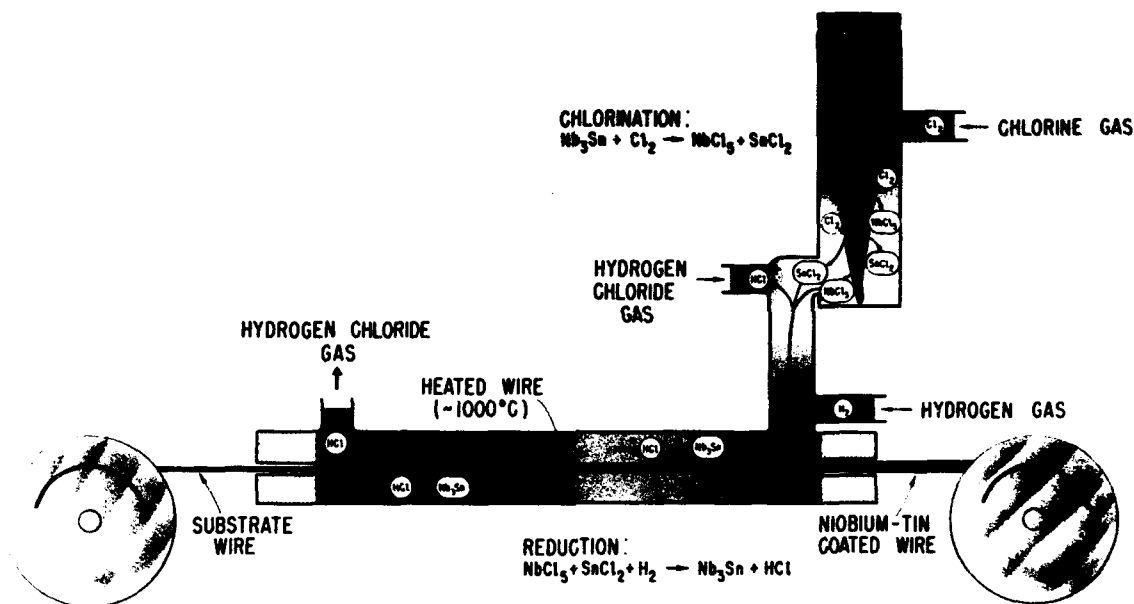
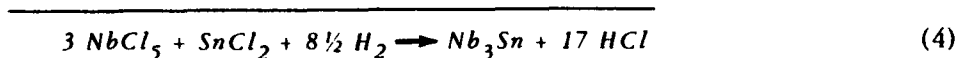
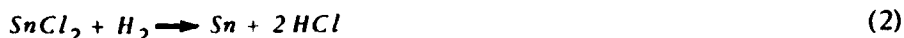


Fig. 7. Schematic diagram for continuous vapor deposition of niobium stannide wire or ribbon.

The vertical chlorination chamber is located in a furnace maintained at 1050 to 1100°C, because it was found that at this temperature, with the apparatus geometry and gas flows used, a stoichiometric conversion of the metals to  $NbCl_5$  and  $SnCl_2$  occurred. The deposition chamber is located in a furnace maintained at 720 to 740°C.

The first attempts to find a suitable temperature at which to maintain the apparatus failed because of the formation of a dark, solid substance, presumably  $NbCl_3$ , which formed freely below 700°C. This problem was resolved by the application of the following qualitative thermodynamic arguments:

The overall chemical reaction for the vapor deposition of Nb<sub>3</sub>Sn can be written as the sum of the three following reactions:

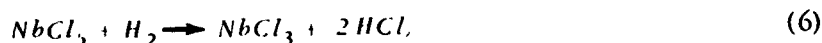


All species in Eq. 4 except Nb<sub>3</sub>Sn are gaseous. Therefore, the equilibrium constant  $K_p$  can be written in terms of the partial pressures  $P_{gas}$  of the gases:

$$K_p = \frac{(P_{HCl})^{17}}{(P_{NbCl_5})^3 (P_{SnCl_2}) (P_{H_2})^{8.5}} \quad (5)$$

The value of  $K_p$  increases monotonically with temperature. Thus, one control over the deposition is achieved by temperature variation. Additional control over the deposition of Nb<sub>3</sub>Sn can be attained by varying the amounts of HCl in the gas stream as indicated by the numerator of Eq. 5, which suggests that the forward reaction (Eq. 4) can be retarded by the addition of gaseous HCl into the gas feed.

A similar situation was encountered with the formation of NbCl<sub>3</sub> which takes place according to the reaction given by Sibert et al (1958),



where

$$K_p = \frac{(P_{HCl})^2}{(P_{NbCl_5})} \quad (7)$$

Equation 7 indicates that the forward reaction can also be retarded by the addition of HCl. It was indeed found that in the range of 720 - 740°C controlled addition of HCl into the gas feed completely prevented the formation of NbCl<sub>3</sub>, and drastically reduced the already slow deposition of Nb<sub>3</sub>Sn on the walls of the apparatus. This allowed for continuous operation of up to 50 hours. The presence of controlled excess of HCl did not prevent the deposition of Nb<sub>3</sub>Sn on the wire surface at approximately 1000-1200°C since the value of the equilibrium constant (Eq. 5) is sufficiently high at this temperature.

Another major factor in the development of the wire process was the selection of the substrate metal. Tungsten and tantalum proved to be unsuitable, because free niobium deposited on them epitaxially prior to the nucleation of the Nb<sub>3</sub>Sn phase. A cross section of such a deposit is shown in Fig. 8a. Large cracks are seen in the Nb<sub>3</sub>Sn phase, and a low rate of nucleation of Nb<sub>3</sub>Sn is manifested by discrete bundles of Nb<sub>3</sub>Sn crystals radiating from distinct points on the

outer surface of niobium. These results indicated that substrates with  $\beta$ -tungsten structure were desirable to aid in the nucleation of  $Nb_3Sn$ . Such substrates are not commercially available. Hence, refractory metal substrates were considered which react with niobium to form  $\beta$ -tungsten compounds. Five metals belong to this category; they are rhodium, osmium, iridium, platinum and gold as indicated by Nevitt (1958). When platinum wire was used as a substrate a single-phase deposit of  $Nb_3Sn$  was obtained, as shown in Fig. 8b. The columnar growth radiating from the substrate exhibits a preferred orientation in the [200] direction normal to the surface. The width of the columns determined by an electron microscope ranges between 750 and 1500 Å, indicating a high rate of nucleation (approximately  $10^5$  nuclei per cm of the surface).

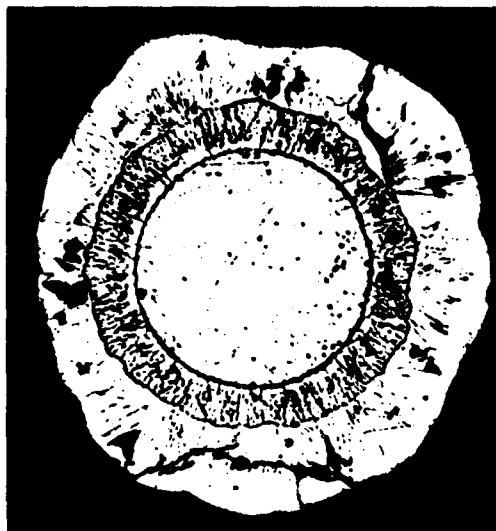


Fig. 8a. Vapor deposition of niobium stannide on tantalum wire (inner deposit is niobium stannide). Wire substrate diameter = 0.018 cm.

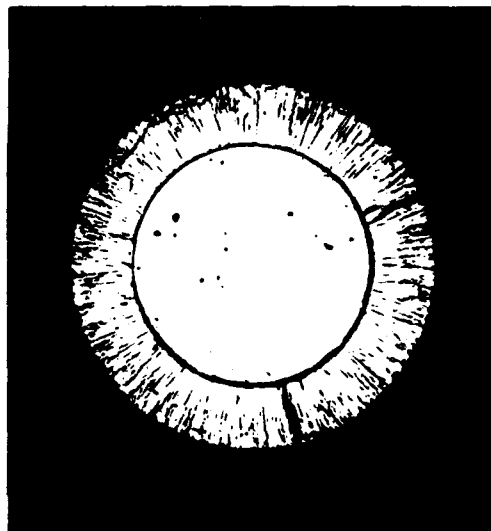


Fig. 8b. Niobium stannide on platinum wire. Wire substrate diameter = 0.018 cm.

Additional examples of the nucleation process are shown in Fig. 9a and 9b for  $Nb_3Sn$  deposit on nickel (which does not form a  $\beta$ -tungsten structure with niobium) and gold-plated nickel ribbons, respectively. A striking similarity can be seen between the deposit on platinum (Fig. 8b) and gold (Fig. 9b), which strongly indicates that  $Nb_3Sn$  growth is preceded by the formation of  $\beta$ -tungsten structure compounds,  $Nb_3Pt$  and  $Nb_3Au$ .

In addition to their role in the nucleation, the noble metals have favorable expansion coefficients, which are slightly larger than that of  $Nb_3Sn$ , thereby giving rise to "prestressed"  $Nb_3Sn$  deposit as the wire is cooled from its deposition temperature to ambient temperature.

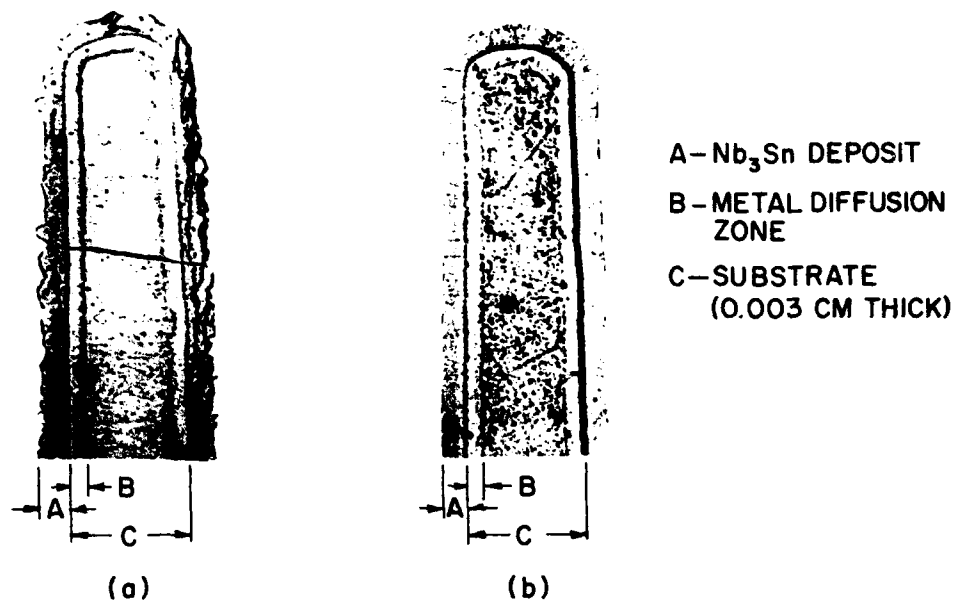


Fig. 9. Niobium stannide vapor deposited on (a) nickel, (b) gold-plated nickel.

#### D. THE DEPOSITION OF $Nb_3Sn$ ON INSULATING SUBSTRATES

There are many areas of application where it is necessary to have  $Nb_3Sn$  without the presence of any other metal. One obvious example is in ac magnetic field generation (as in many proposed plasma devices) where the presence of an extraneous metal would result in unnecessary and deleterious heating due to eddy currents. Apart from application, there is clearly the need for insulator-deposited films of  $Nb_3Sn$  for fundamental research. Electrical measurements can only be complicated by the presence of another metal. Furthermore, many experiments are only possible with either insulator deposited  $Nb_3Sn$  films or unsupported films, e.g., infrared and Mössbauer experiments. Finally it has been experimentally and theoretically shown that for sufficiently thin layers of a superconductor, a metallic substrate can reduce or even destroy the superconductivity of the deposit. (Parmenter, 1960; Shapiro et al 1961). Thus the very interesting area of  $Nb_3Sn$  films with thickness considerably less than the penetration depth (see Section B) can only be approached through the medium of insulator deposits.

For the above reasons, an RCA-supported program on the deposition of  $Nb_3Sn$  on insulators was inaugurated, and some of the more interesting results are described here. Some experiments made on insulator-deposited specimens are described here and in Section III-E.

To show the range of application of static depositions on a ceramic, several illustrations are given. The deposition technique is similar to the process described in previous reports, and will not be discussed further.

Figure 10 shows the  $Nb_3Sn$  on a flat ceramic substrate (a) as deposited and (b) subsequent to polishing. The material can be polished to a mirror finish. Figure 11 shows a polished deposit



Fig. 10. Polished Nb<sub>3</sub>Sn on ceramic flats.



Fig. 11. Polished Nb<sub>3</sub>Sn deposit on a ceramic cylinder.

on the exterior of a ceramic tube. Patterns may be made in the deposited material by several methods. The strip in Fig. 12 has been formed simply by chemical dissolution of unwanted material starting with a completely coated wafer. The spiral deposit in Fig. 13 was formed as follows: A spiral recess was machined in the ceramic substrate;  $Nb_3Sn$  was then deposited over the entire wafer; and finally, the deposited material was ground away until only the recessed spiral remained. A duplicate spiral has been placed on the opposite side, and contact is made with  $Nb_3Sn$  deposited in the hole in the middle.



Fig. 12.  $Nb_3Sn$  sample with current and potential leads.

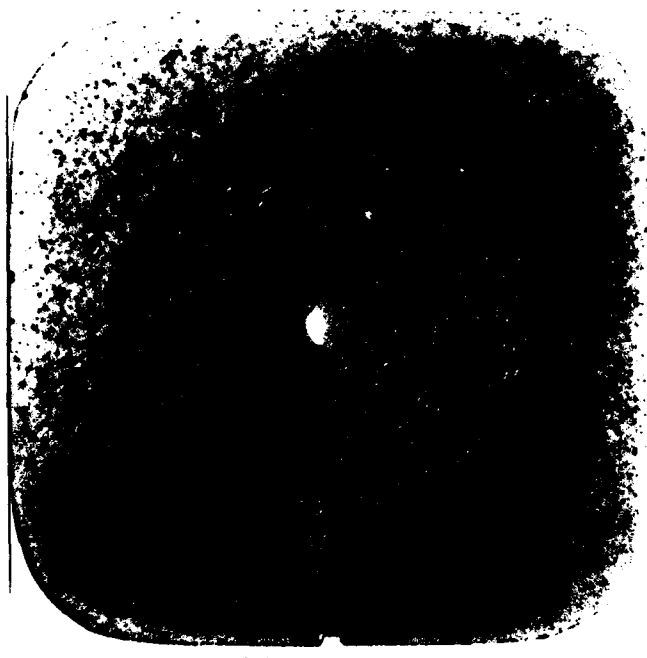


Fig. 13.  $Nb_3Sn$  deposit in a spiral groove of a ceramic flat.



It is planned to use these and other geometries for ac critical current measurements, persistent current measurements, magnetization experiments, penetration depth measurements, and infrared reflectivity measurements. Although further work is required to improve the uniformity of these deposits, it is believed that the present specimens are suitable for these experiments.

Since this deposition is static, it is possible to control the composition rigidly. It is planned to use these static depositions as a tool to further explore the effect of composition and disorder on the superconducting properties of niobium stannide. Finally, since the ceramic can be chemically etched without harming the deposit, the process lends itself to the production of unsupported films of Nb<sub>3</sub>Sn.

The ultimate aim of the present research is the production of very thin films of Nb<sub>3</sub>Sn, and a good deal of further research is necessary to produce uniform films in the range of thickness less than a micron.

### E. PHYSICAL PROPERTIES AND CHEMICAL ANALYSIS

Some of the physical properties of vapor-deposited niobium stannide appear in Table II. The purity of the vapor-deposited Nb<sub>3</sub>Sn was higher than that of the starting sintered material with respect to all nongaseous impurities. The nongaseous impurity level of statically deposited crystals and the continuously deposited wire or ribbon were comparable except for silicon, which was present in amounts of 300-5000 ppm in the deposited crystals (the same or greater than in the starting materials) and only a few parts per million in the deposited ribbon. The reason for the difference is that in the case of the static process both the gases and the deposit have a much greater chance of reacting with the quartz apparatus than in the case of the ribbon deposition.

TABLE II

SOME PHYSICAL PROPERTIES OF VAPOR-DEPOSITED NIOBIUM STANNIDE

Nature of deposit .....	Single-phase, $\beta$ -tungsten structure
Lattice constant range .....	5.284 — 5.289 Å
Composition range .....	76.2 to 81.5 atomic percent Nb
Macroscopic density .....	8.80 g/cm <sup>3</sup>
Lattice disorder .....	20 — 100 percent
Coefficient of expansion (20-1000°C) .....	$7.1 \times 10^{-6} (\text{°C})^{-1}$
Modulus of elasticity .....	$9 \times 10^6$ psi*
Tensile strength .....	24,000 psi*
Resistivity (300°K) .....	$12 \times 10^{-5}$ (ohm-cm)

\*Tentative values only.

Analytical results obtained with the emission spectrograph were given in a previous report [RCA (1961)]. Mass spectrographic results on one ribbon specimen are given in Table III. These data reveal a high concentration of the gaseous impurities, namely, hydrogen, chlorine, carbon and oxygen.

TABLE III  
 MASS SPECTROGRAPH (MS 7) ANALYTICAL RESULTS FOR  
 VAPOR-DEPOSITED NIOBIUM STANNIDE RIBBON

ELEMENT	CONCENTRATION IN PPM (ATOMIC)	
	Nb <sub>3</sub> Sn on Pt	Pt Substrate
H	9,000	3,000
B	12	12
F	1.2	1.2
Na	120	12
Mg	9	10
Al	36	12
Si	15	165
P	5	15
S	15	5
Cl	1,560	15
Ti	5	1.5
V	0.4	1.2
Cr	55	5.4
Mn	1.5	1.5
Fe	45	45
Ni	6	6
Cu	130	130
Zn	15	15
Ga	0.5	0.2
Ge	0.07	23
As	3	3
Sr	0.04	0.04
Zr	2	2
C	3,000	450
N	140	12
O	1,000	1,350
Nb	<i>strong</i>	1,500
Mo	0.3	12
Ru	60*	18
Rh	1,200*	1,200
Pd	120*	120
Ag	60	200
Cd	0.2	0.2
Sn	<i>strong</i>	6,800
Sb	2.5	0.8
Ta	3	1
W	0.1	---
Ir	51*	51
Pt	<i>strong</i>	<i>strong</i>
Pt	100 - 1000+	
Au	10	10

\* Noble metals are probably not in the deposit in these amounts; they appear because of the substrate (see Pt result).  
 + Emission spectrographic result. Pt substrate removed by etching.

Included are data on the platinum substrate ribbon from which niobium stannide had been etched off. Chemical analyses for tin and niobium were done by means of an X-ray fluorescence technique in which sintered materials were used for calibration. Single-phase,  $\beta$ -tungsten structure deposits on wire and ribbon substrates had compositions ranging between 76.2 and 81.5 atomic percent niobium because of changing conditions in the deposition process. This composition range is in a close agreement with the phase diagram proposed by Wyman et al (1962), who have shown that in the niobium-tin system above 863°C only one compound exists with very nearly the same composition range as that given above.

## F. CRITICAL CURRENT DATA

Critical current measurements as a function of magnetic field were made on wires and ribbons with the cross-sectional area of niobium stannide ranging from  $5 \times 10^{-5}$  to  $2 \times 10^{-4}$  cm<sup>2</sup>. Preliminary results reported previously by Hanak et al (1961) were comparable to published results for sintered materials reported by Kunzler (1961). With recent modifications in the deposition process and the technique of establishing current contacts (total contact resistance =  $3 \times 10^{-5}$  ohm), significant improvements in the critical current density ( $J_c$ ) were realized. These results are shown in Fig. 14, which gives  $J_c$  data on vapor-deposited ribbon as a function of transverse dc field measured by Aron and Hitchcock (1962 a) up to 93.5 kgauss. These data are given for ribbons with  $T_c$  of 17.6°K and 14.6°K. The  $J_c$  for the ribbon with  $T_c$  of 14.6°K is significantly the lower of the two; but even here the characteristic "knee" in the  $J_c$  curve is not approached at the maximum field. Figure 14 further shows published data for sintered Nb<sub>3</sub>Sn wire by Kunzler (1961). Finally, measurements in a pulsed, longitudinal field of 170 kilogauss by Cherry made at RCA indicate  $J_c$  of  $1.5 \times 10^5$  amp/cm<sup>2</sup> for a wire with  $T_c$  of 17.5°K.

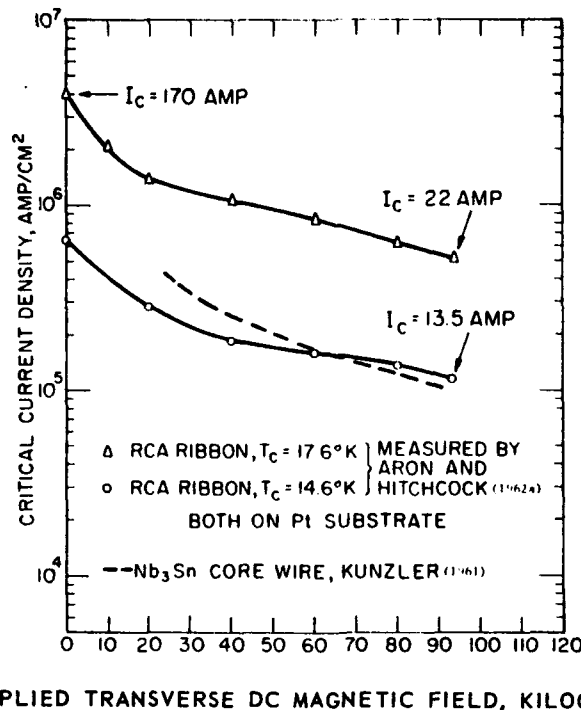


Fig. 14. Critical current as a function of applied transverse field.

The variation in the critical current density was measured in more detail at lower transverse dc fields for ribbons ranging in  $T_c$  from 8.2 to 17.6°K. In Fig. 15 data are shown on  $J_c$  as a function of transverse dc field for vapor-deposited ribbons of variable  $T_c$ . The actual currents ranged from 2 to 98 amps, and the contact resistance ranged from  $8 \times 10^{-5}$  ohms for low  $J_c$

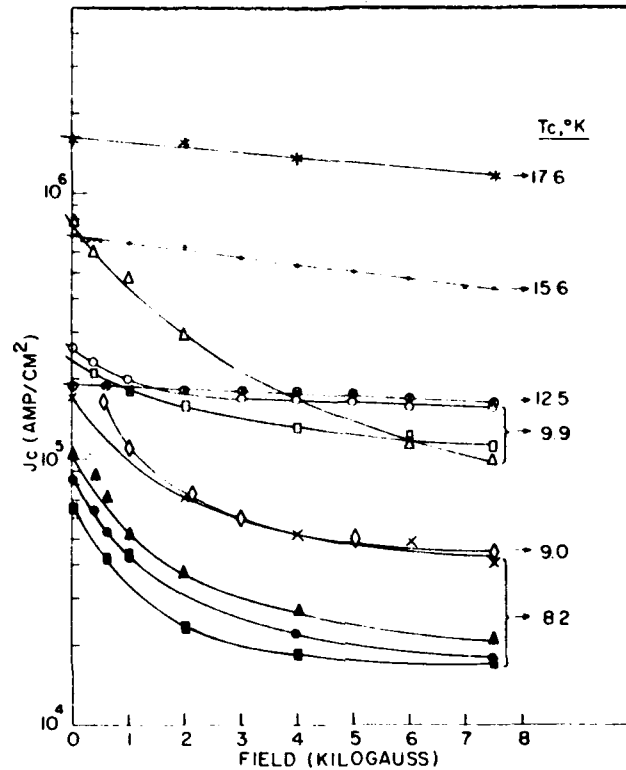


Fig. 15. Critical current density vs. transverse field for vapor-deposited niobium-tin with variable  $T_c$ .

materials to  $2 \times 10^{-5}$  ohms for high  $J_c$  materials. Of the two types of  $J_c$  vs.  $H$  curves the linear ones predominate at higher  $J_c$ , while the hyperbolic ones predominate at lower  $J_c$ . These differences are believed to arise from still inadequate current contacts which become especially detrimental at high currents. The chief characteristic of the  $J_c$  vs.  $H$  curves in Fig. 15 is that at a magnetic field of 7500 gauss  $J_c$  increases rapidly with increasing  $T_c$  according to the expression:

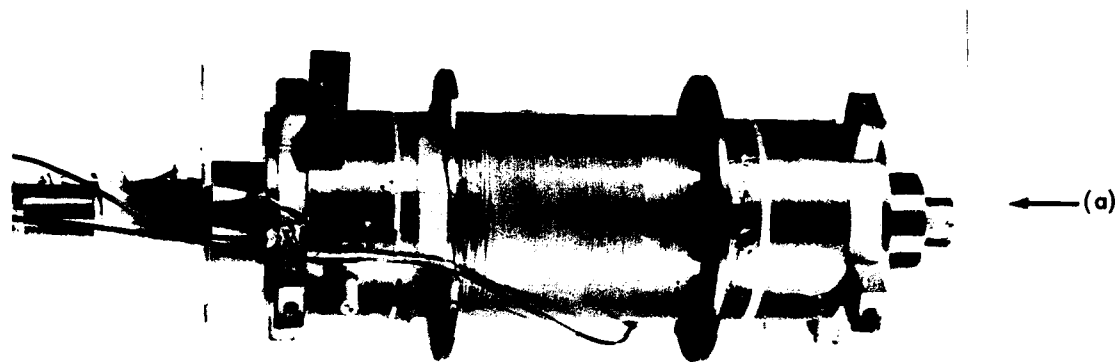
$$\log J_c = 0.164 T_c + 3.16 \quad (8)$$

Although its theoretical significance is not known, this behavior is noteworthy since it relates  $J_c$  over a long range of  $T_c$  for materials which are nearly identical from the standpoint of structure and chemical composition, thereby eliminating the influence of these parameters.

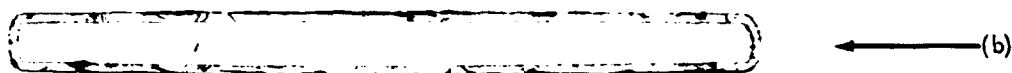
### G. $\text{Nb}_3\text{Sn}$ SOLENOID

To demonstrate the usefulness of vapor-deposited niobium stannide in the construction of solenoids, coated ribbon, rather than the wire, was used because of its better mechanical properties, more convenient handling and higher packing factor. Typical cross-sectional dimensions of the ribbon substrate made of platinum are 0.070 cm by 0.0037 cm with the thickness of the  $\text{Nb}_3\text{Sn}$  deposit ranging from 0.0003 to 0.0010 cm.

Three sections of such ribbon totalling 450 meters have been wound into a solenoid. The solenoid form was made of an aluminum bronze alloy (Duronze 708), such that the coil had an inside diameter of 5.1 cm, outside diameter of 6.0 cm and a length of 6.3 cm. The ribbon was uninsulated except for a thin oxide coating, which allows for only resistive contacts, and 0.0006 cm thick Mylar sheet between consecutive layers. Figure 16 is a photograph of the first section of the solenoid and a cross-sectional view of the ribbon used. The performance characteristics are given in Table IV.



(a) FIRST OF THREE SECTIONS OF A 10,360 GAUSS SOLENOID WOUND WITH VAPOR-DEPOSITED NIOBIUM STANNIDE RIBBON.



(b) CROSS SECTIONAL VIEW OF THE RIBBON USED -  
- 0.072 CM  $\times$  .0055 CM,  
DEPOSIT THICKNESS - 0.0008 CM.

Fig. 16.  $\text{Nb}_3\text{Sn}$  solenoid with cross section of tape.

**TABLE IV**  
**PERFORMANCE OF  $Nb_3Sn$  SOLENOID**

SECTION	NO. OF TURNS	QUENCHING* CURRENT (AMP)	$J_c$ (AMP/CM <sup>2</sup> )	FIELD OBSERVED	FIELD CALCULATED
Inside	552	35	$2.5 \times 10^5$	----	----
Middle	930	17	$1.4 \times 10^5$	10,360	11,300
Outside	1256	32	$2.7 \times 10^5$	----	----

\* At 10,300 gauss, all sections operating in parallel. At the same field the  $J_c$  of short test pieces of ribbon was  $3.2 \times 10^5$  to  $4.0 \times 10^5$  amp/cm<sup>2</sup>. The  $T_c$  of the ribbon ranged from 14.6 to 15.8°K.

The solenoid was operated repeatedly both with and without protective shunts placed in parallel with each section and through numerous current quenches and temperature cyclings. The so-called "training effect" was not experienced. The observed range of current densities (see Table IV) represents the highest  $J_c$  for a superconducting solenoid reported to date.

By comparison  $Nb_3Sn$  sintered wire in solenoids has operating current densities between  $5 \times 10^4$  and  $1 \times 10^5$  amp/cm<sup>2</sup> reported by Salter et al (1961), whereas Nb-Zr wire solenoids operate at maximum current densities of up to  $5 \times 10^4$  amp/cm<sup>2</sup> obtained by Hulm (1962). The larger the current density, the less wire is needed to construct a solenoid and, hence, the more compact the solenoid. The same length of Nb-Zr wire carrying its usual 19 amperes would produce a field of 7,300 gauss.

## IV. PROPERTIES OF Nb<sub>3</sub>Sn

### A. EFFECT OF LATTICE DISORDER ON THE TRANSITION TEMPERATURE OF NIOBIUM STANNIDE

The compositional variation of vapor-deposited niobium stannide described above results in significant changes in  $T_c$ , as shown in Fig. 17, where the variation of  $T_c$  with composition is shown for vapor-deposited materials. For comparison, Fig. 17 also includes data on "twice-sintered" specimens reported by Jansen and Saur (1960). Striking differences are seen between the sintered and the vapor-deposited materials indicating that composition (or electron-to-atom ratio) is not sufficient to describe the variation in  $T_c$ .

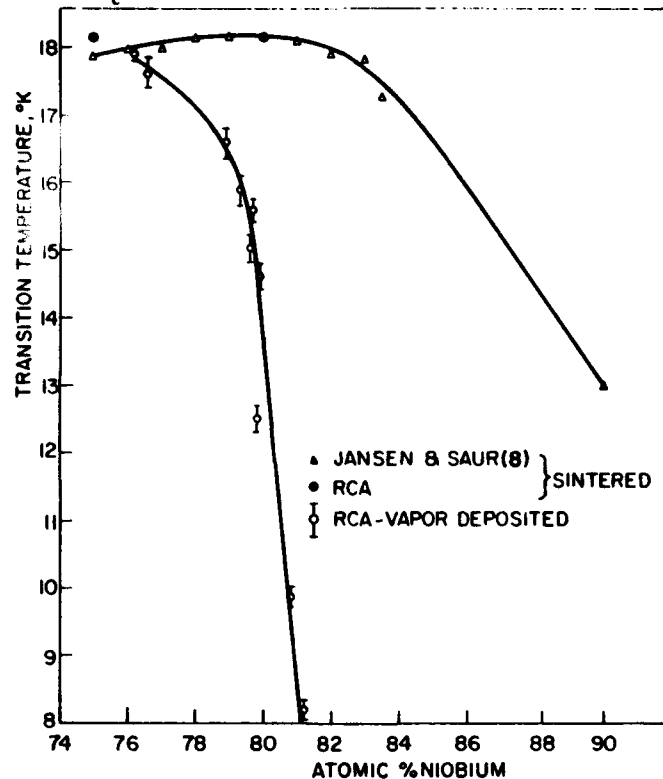


Fig. 17. Transition temperature vs. composition of  $\beta$ -tungsten Nb-Sn.

It was reported previously by Hanak et al (1961) that extensive lattice disorder had been observed in the vapor-deposited niobium stannide. This disorder is of the type where niobium occupies normal tin sites, or the converse. To determine whether this disorder could account for the difference in  $T_c$  between sintered and deposited niobium stannide, shown in Fig. 17, measurements of disorder were made from the intensity ratio of the (210) and (211) X-ray diffraction lines.\* Although disorder was small for both vapor-deposited and sintered materials with

\* For ordered Nb<sub>3</sub>Sn this ratio is 1.037, and for the disordered compound it is 1.330. The value of 0.963 for the ordered lattice reported previously by Hanak et al. (1961) was found to be in error.

compositions near 75% niobium material the deposited specimens exhibited extensive disorder, while a sintered specimen exhibited essentially complete order. These data clearly suggest that disorder is connected with the observed differences in  $T_c$  shown in Fig. 17; however, this connection needs to be defined.

With materials having variable composition it is more useful to speak of lattice site occupancy than of percent disorder. This is illustrated in Fig. 18, where theoretical lines are drawn defining lattice site occupancy for the  $\beta$ -tungsten structure in the composition range between

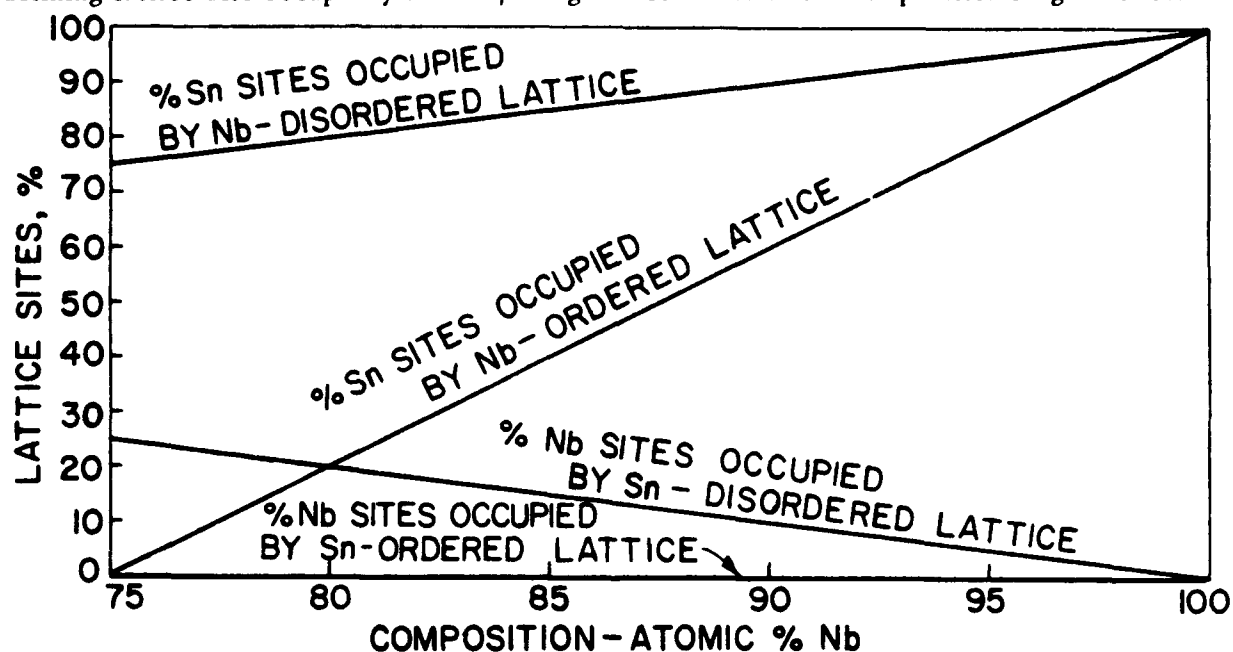


Fig. 18. Lattice site occupancy-composition for ordered and disordered niobium-tin.

75 and 100% niobium, and for completely disordered and completely ordered lattice.\* It can be seen from the calculated curves in Fig. 18 that the occupancy of niobium sites by tin for both the ordered or disordered cases is of little consequence. In support of this, experimental data showed only  $9 \pm 5\%$  occupancy of niobium sites by tin over the entire composition range.

In the case of tin sites being occupied by niobium, Fig. 18 shows that it can vary from 0 to 100% over the composition range under consideration. For the ordered lattice the occupancy of the tin sites by niobium can be extensive only at high niobium compositions. This is the case encountered with the sintered specimens. However, for the disordered or partially disordered lattice, extensive occupancy of the tin sites by niobium can be achieved even at 75% niobium composition. This strongly suggests that the occupancy of the tin sites is responsible for the observed differences in  $T_c$  between the sintered and the vapor-deposited specimens. This is clearly demonstrated by the linear relation in Fig. 19, which shows that the dependence of  $T_c$  on tin site occupancy is nearly the same for both the sintered and vapor-deposited specimens, although their respective compositions

\* In this discussion the lattice is completely ordered when the niobium sites are occupied entirely by niobium, and completely disordered when all sites have the same average occupancy equivalent to the chemical composition.



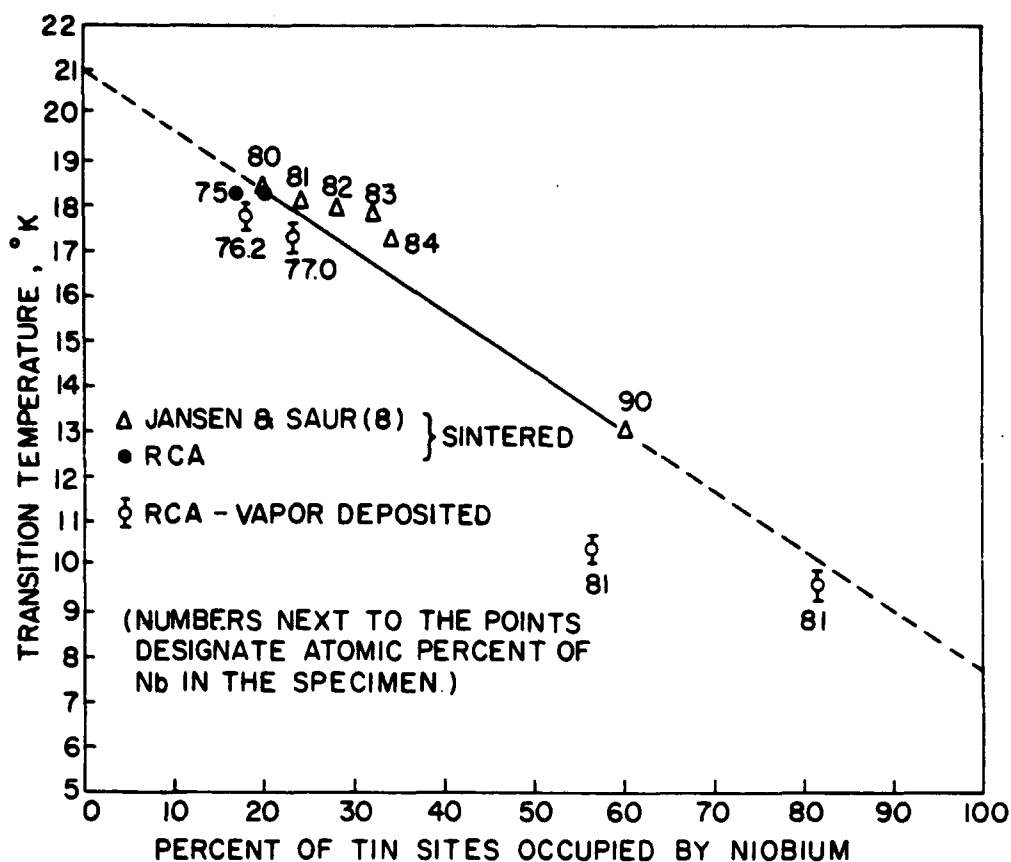


Fig. 19. Transition temperature vs. percent of tin sites occupied by niobium for  $\beta$ -tungsten Nb-Sn.

differ largely. The tin site occupancy by niobium for the sintered specimens was determined from Fig. 18 assuming that specimens with niobium content greater than 80% are ordered, because the specimen with 80% niobium is ordered. The straight line drawn is for the sintered specimen. For the vapor-deposited specimens all values of tin site occupancy were determined experimentally.

In vapor-deposited niobium stannide the occurrence of extensive lattice disorder is believed to represent a metastable state of the lattice, because specimens sintered at the same temperature as that of the deposition reaction are essentially ordered. The cause of disorder in the vapor-deposited specimens is attributed to the reaction kinetics; i.e., a rapid growth rate (2 minutes for vapor deposition vs.  $\sim 20$  hours for sintering), combined with appropriate chemical conditions. Therefore, it appeared that the lattice disorder should be removed by long time annealing.

A specimen of vapor-deposited niobium stannide having low transition temperature was therefore annealed for 67 hours at 1100°C in vacuo. The composition of the specimen determined by X-ray fluorescence was found to be 80.6 atomic percent niobium and 19.4 percent tin\* ( $\text{Nb}_{4.1}\text{Sn}$ ).

\* Only relative amounts of niobium and tin were determined by this method, regardless of impurities.

The lattice disorder and the transition temperature were determined for both the annealed and unannealed specimens, and the data are given in Table V.

TABLE V  
LATTICE DISORDER AND  $T_c$   
OF UNANNEALED AND ANNEALED  
VAPOR-DEPOSITED NIOBIUM STANNIDE,  $Nb_{4.1}Sn$

SPECIMEN	$T_c$	PERCENT OF TIN SITES OCCUPIED BY NIOBIUM		
		OBSERVED	ORDERED LATTICE	DISORDERED LATTICE
Unannealed	7.0	35.7	22.4	80.6
Annealed	16.0	22.5		

The data in Table V indicate that annealing essentially removed lattice disorder in the specimen, and raised  $T_c$  as expected. However, the unannealed specimen had much less disorder than previously observed with specimens having low  $T_c$ . There is a possibility that dissolved hydrogen (see Table III) adds to the lowering of  $T_c$ ; this possibility will be investigated further.

#### B. RESISTIVITY OF DEPOSITED $Nb_3Sn$

Until the past year,  $Nb_3Sn$  has been available only in a sintered form. Sintered polyphase  $Nb_3Sn$  had been sufficient to give information on the superconducting properties of this material, in particular its high superconducting transition temperature and its ability to support high current densities in very high magnetic fields. The striking superconducting characteristics of  $Nb_3Sn$  have emphasized the importance of further information on its properties. Unfortunately, sintered material has been useless for all but gross effects. Recent developments in the preparation of this material have made less crude measurements possible for the first time. One now has available single-phase crystalline deposits on both metals and insulators suitable for precise electrical and magnetic measurements in both the superconducting and normal state.

The present section concerns resistivity measurements made from 4.22°K to 373.7°K on a sample made of  $Nb_3Sn$  deposited on an insulator. The deposit was polished to a thickness of  $\approx 5.1 \times 10^{-3}$  cm, was  $1.88 \times 10^{-1}$  cm wide and had a 1.69 cm separation between potential contacts. This sample, G-35, had been used for tunneling experiments and had a similar resistivity as sample G-35-1. The major uncertainty in determining the resistivity is the thickness determination. At the present, this leads to an absolute uncertainty of  $\pm 10\%$ . Temperatures were measured with respect to a helium gas thermometer calibrated with respect to liquid oxygen and liquid helium; potential measurements were made with a Leeds and Northrup K-3 potentiometer.

The results of these measurements are shown in Fig. 20, where the resistivity is plotted as a function of temperature. The form of the curve is best approximated in the temperature range

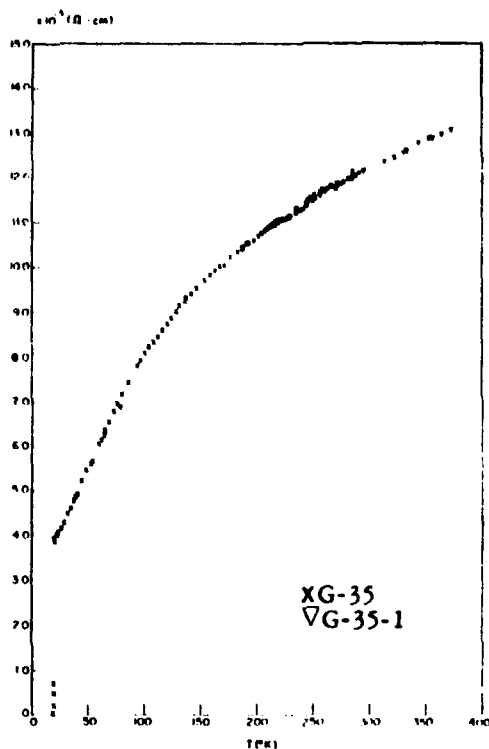


Fig. 20. Resistivity of Nb<sub>3</sub>Sn.

considered (4.2°K – 370°K) by

$$\rho = 2.75 \times 10^{-5} + 6 \times 10^{-7} T (1 - 1.56 \times 10^{-3} T),$$

where  $\rho$  is in ohm-cm and  $T$  is in degrees absolute. The present results are in qualitative agreement with previous resistivity measurements made on sintered Nb<sub>3</sub>Sn and small deposited films of Nb<sub>3</sub>Sn (RCA, 1961). The differences in shape and absolute value can be ascribed to different residual resistivity, and geometrical uncertainties in obtaining absolute resistivities from measured resistances for previous samples.

The significance of the present results is in the removal of any remaining uncertainty in the previous resistivity measurements. Nb<sub>3</sub>Sn appears to be unique among metals in that it has a very high resistivity at 300°K and a strong nonlinear temperature dependence below 300°K. This temperature dependence should be contrasted with high resistance alloys or semimetals where there is very little temperature dependence.

In previous reports under this Contract (RCA, 1961) several mechanisms that could be responsible for this resistivity temperature dependence were discussed. It was decided that a reasonable explanation could be based either on the presence of bound states, or a low degeneracy temperature. The present experiment has only reinforced the preliminary observations and has considerably increased the accuracy. It is still necessary to examine other properties of Nb<sub>3</sub>Sn to

determine the explanation of the resistivity curve, and to relate it to the similarly unique low temperature properties of  $Nb_3Sn$ .

### C. TUNNELING IN SUPERCONDUCTING $Nb_3Sn$

Current-voltage characteristics at 4.2°K have been obtained for the sandwich structure:  $Nb_3Sn-Nb_3Sn$  oxide – and various normal metals. The curves shown are to be taken as representative, rather than final, since all of the current measured is clearly not all due to tunneling. These results are interesting, however, since they shed light on the behavior of the shorting mechanism when an imperfect oxide is used; and they strongly suggest that an energy gap exists in superconducting  $Nb_3Sn$ .

Two forms of polycrystalline  $Nb_3Sn$  have been available for study:  $Nb_3Sn$  deposited on a non-superconducting metal ribbon and on a ceramic substrate. The former cannot be conveniently polished, while the latter has been mechanically polished to a mirror finish. Surprisingly, our results have been independent of the form of  $Nb_3Sn$ ; i.e., an experimental curve of each type, shown in Fig. 21, has been obtained on both ribbon and polished platelets. The oxide has been

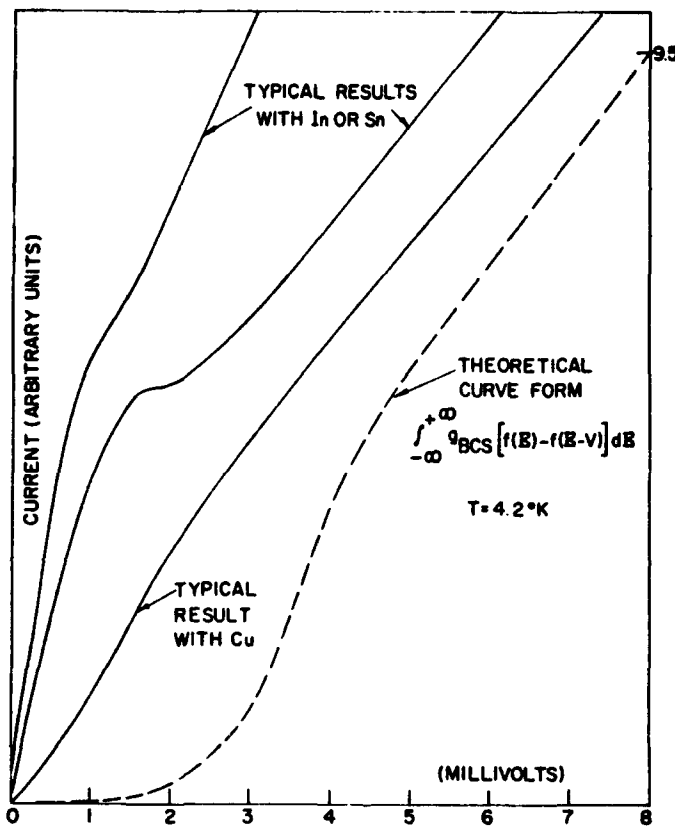


Fig. 21. I-V characteristics of  $Nb_3Sn$  tunnel diodes.

taken to be adequate as typical junction resistances are in the range 10-100 ohms. It remains to be shown that the ideal tunneling behavior can be reached by an appropriate formation of the perfect insulating barrier. The normal metals have been vacuum evaporated over the Nb<sub>3</sub>Sn oxide which is mounted in an insulating epoxy whose expansion coefficient matches that of the metals well enough to allow temperature cycling of the specimen. The general characteristic for a particular sample is reproducible, while the specific details are not. A progression toward higher conductance is seen with temperature cycling. The thickness of the Nb<sub>3</sub>Sn ranged from 5 to 50 microns which places these specimens in the category of bulk superconductors. Current and voltage leads are separate, as in Giaever's experiment (Giaever and Megerle, 1961); and measurements are made with an x-y recorder whose input impedance is much greater than the resistance of the junctions.

With indium or tin as the normal metal, the characteristics are generally like the two upper curves shown in Fig. 21. It is clear that the In and Sn films are not completely superconducting over the junctions at 4.2°K, because the reduction in temperature below the transition temperature of In or Sn results in a superconducting short. The large positive conductance at low voltages for Sn and In on Nb<sub>3</sub>Sn at 4.2°K is, therefore, interpreted as due to a partial superconducting short. The nature of the short may be assumed to move the superconducting-normal interface closer to the bulk of the normal metal. As the currents through the shorts are increased, the total resistance of the filament increases and gives rise to a high resistance region on the I-V characteristic. Non-zero conductance at low voltages has been observed in tunneling into bulk niobium (Sherrill and Edwards, 1961), and has been reported elsewhere (Shiffman, 1961) for tunneling into bulk superconductors. To test this hypothesis for the extra current, one may ask: What normal metal will minimize the shorting effects? If the establishment of partial superconductivity in the filamentary shorts is due to the enhancement of the superconductivity (Meissner, 1960) of the Sn or In by the Nb<sub>3</sub>Sn, then replacement of Sn or In by a metal such as Cu should reduce the magnitude of the extra current. A result with Cu which is representative of both types of Nb<sub>3</sub>Sn (polished and rough surface) is also shown in Fig. 21. The curvature at very low voltages is now more nearly that of the ideal tunneling curve. All the nonlinearities are associated with the superconductivity of Nb<sub>3</sub>Sn, since the curves without exception have been linear just above the transition temperature of Nb<sub>3</sub>Sn. The initial junction resistance for In and Sn is typically 20% greater at 300°K than the resistance at 4.2°K (for large voltages). In the case of Cu it is equal. A theoretical curve is calculated from the expression given for the tunneling current from a normal metal into a superconductor. The parameters of the calculation are

$$2E_0 = 3.5k18.0 (^{\circ}K); T = 4.2^{\circ}K; g_{BCS} = \frac{E}{E^2 - E_0^2},$$

where  $2E_0$  is the energy gap,  $T$  is the temperature and  $g$  is the density of states from the BCS theory. Fig. 22 shows the normalized density of states for two choices of energy gap parameters at 4.2°K. The dashed line through the dots is associated with the data of Nb<sub>3</sub>Sn-Cu specimen, normalized by its slope at high voltages. The agreement with theory is sufficient to conclude that a gap exists. The transition temperature of the Nb<sub>3</sub>Sn has been measured as  $17.9 \pm 0.1^{\circ}K$ . The BCS theory gives a connecting constant of 3.5 between energy gap and transition temperature, whereas our data suggest a value of about half this for Nb<sub>3</sub>Sn.

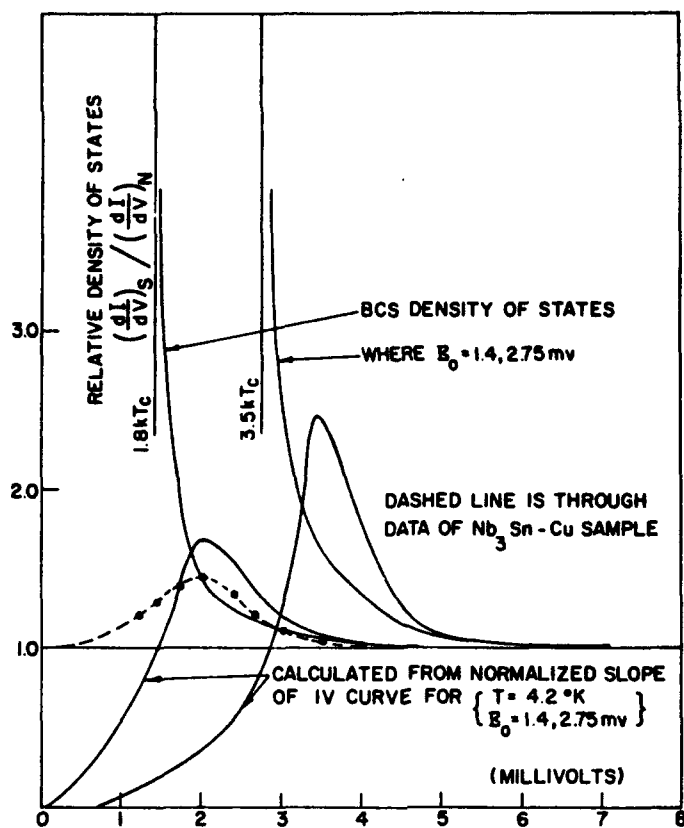


Fig. 22. Relative density of states of  $Nb_3Sn$ .

The existence of an energy gap has been experimentally verified for  $Nb_3Sn$  with a value of  $1.8kT_c$ . This value may be a lower limit because of possible anisotropy in the gap and the effect of shorting to the Cu (Parmenter, 1960). Also, it is clear that the importance of pin-hole shorts, for the determination of an energy gap, can be minimized by using a metal which is not likely to become a superconductor even at lowest temperatures.

#### D. PENETRATION DEPTH OF $Nb_3Sn$

Measurements have been made of the change in penetration of a longitudinal magnetic field of variable peak amplitude and frequency into specimens of  $Nb_3Sn$  over the temperature range, 4.2°K to 18.2°K. The specimens consist of wires of a nonsuperconductor coated with a chemically deposited layer of  $Nb_3Sn$  (Hanak, 1962). Chemical and metallurgical analysis of the individual wires showed the deposit to have the form of a smooth (to  $\approx 10^{-4}$  cm) circular cylinder of single-phase  $Nb_3Sn$  oriented with the (200) plane parallel to the wire axis. The sample discussed in detail below (43-4) consisted of 71 wires of length  $2.1 \pm .4$  cm. The substrate diameter was  $8.98 \times 10^{-3}$  cm; the deposit thickness was  $5.6 \times 10^{-4}$  cm. The transition temperature ( $T_c$ ) of this sample was 17.8°K with a transition width of the order of 1% of  $T_c$ . Figure 23 is a photomicrograph of a cross section of a 43-4 wire. Figure 24 is a larger magnification of the wire. As noted

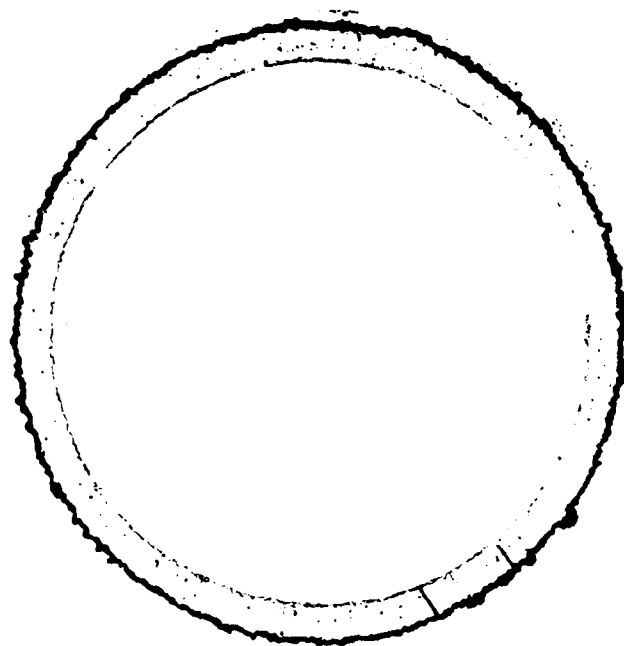


Fig. 23. Cross-section of deposited Nb<sub>3</sub>Sn sample 43-4, magnified 400X. Sample nickel plated and polished, but not etched.

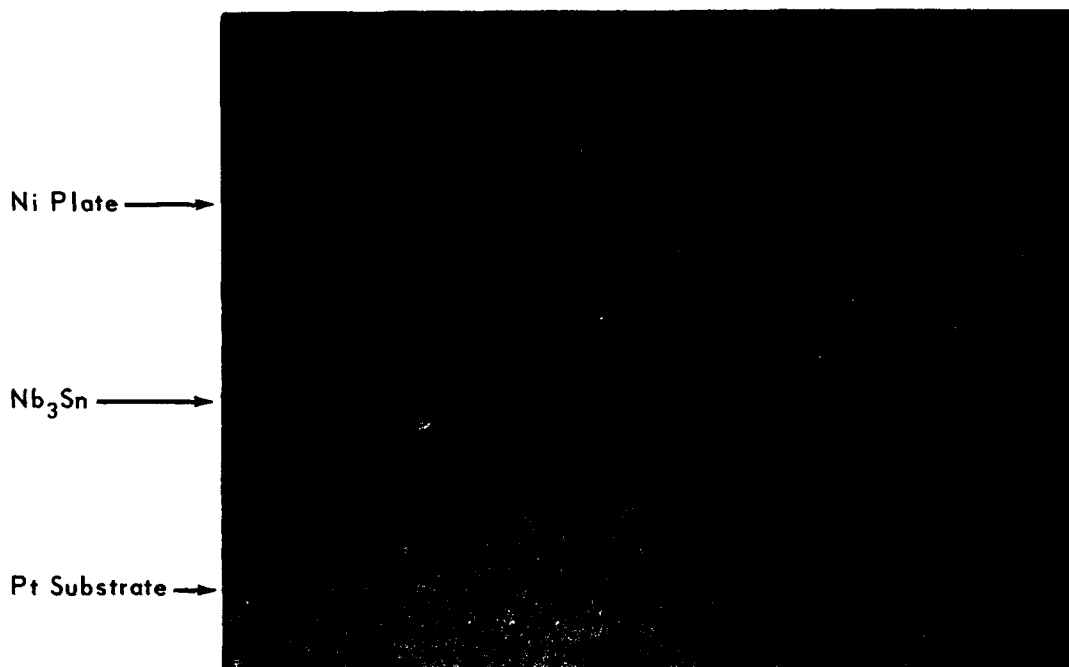


Fig. 24. Cross-section Nb<sub>3</sub>Sn sample 43-4 (2304X magnification).

by Hanak (1962) these materials have properties similar to those of the sintered materials previously available ( $T_c = 18.1^\circ\text{K}$ ;  $\Delta T_c / T_c \approx 3\%$ ), except for the narrow transitions.

The wires were encapsulated in a glass tube with a molybdenum base, and the tube was closed in an atmosphere of 60 cm of helium gas to ensure thermal equilibrium among the wires. A 0.1-watt, 56-ohm carbon resistor was cemented with GE 7031 adhesive into a hole in the molybdenum base 3 mm below the bottom of the wires. The base fitted snugly into a hole in a copper block which was kept in good thermal contact with a gas thermometer by Apiezon N grease. A schematic of the apparatus is shown in Fig. 25. A 41 mh coil, 1.5 cm long, consisting of 4600 turns of AWG No. 40 copper wire, was placed around the glass tube and grounded thermally to the copper block. The coil and sample were isolated from the bath by a vacuum of about  $4 \times 10^{-6}$  mm. The sample isolation was such that without exchange gas in the exchange gas chamber the sample

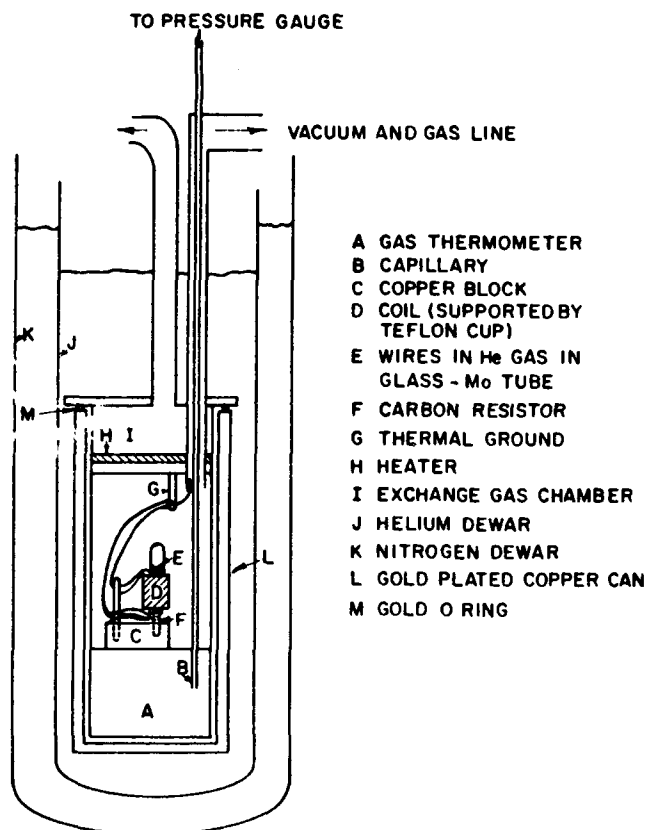


Fig. 25. Schematic of penetration depth apparatus.

rose to  $10^\circ\text{K}$  with no heat input to the heater. The inductance of this coil was measured as a function of temperature with a high sensitivity Anderson Bridge (Bleaney and Bleaney, 1957), where changes of inductance and equivalent resistance for the coil could be measured to a precision of about two parts in  $10^5$  and one part in  $10^3$ , respectively. A schematic diagram of the bridge is shown in Fig. 26. The temperature was measured with the carbon resistor calibrated



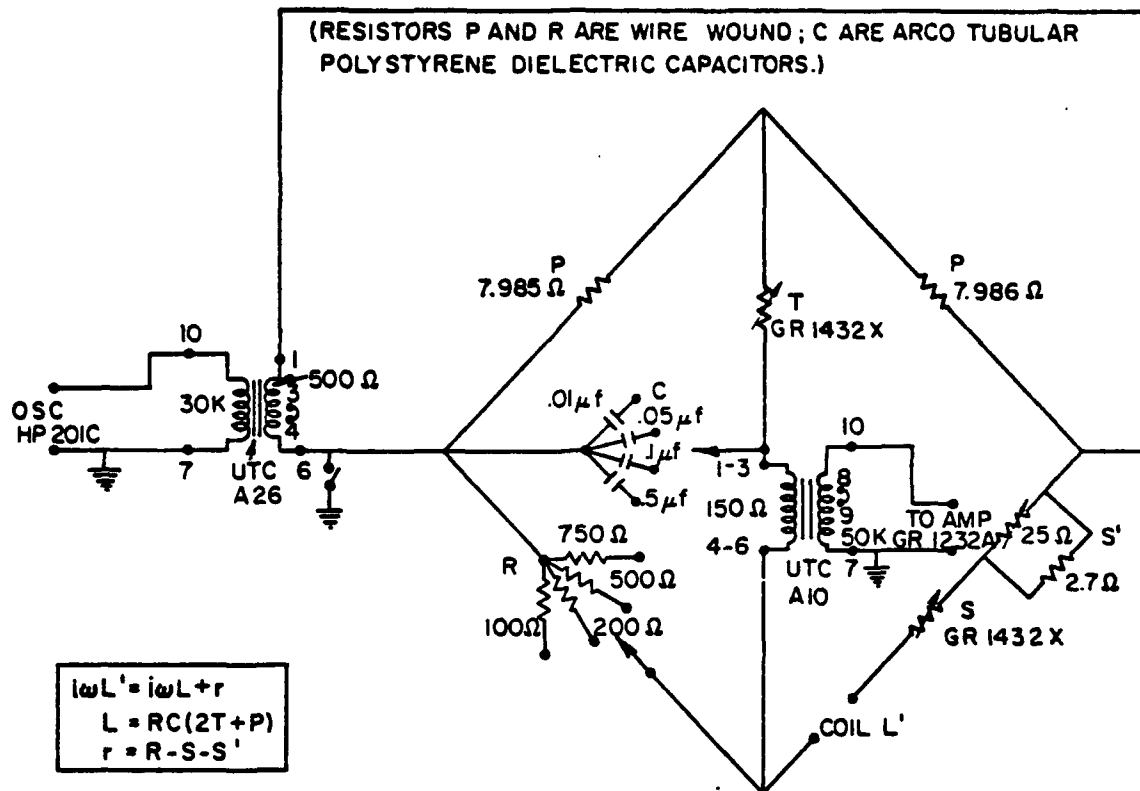


Fig. 26. Anderson inductance bridge.

with respect to the vapor pressure of liquid helium and a point at 18.21°K determined by the gas thermometer, which in turn was calibrated with respect to the vapor pressures of liquid helium, nitrogen and oxygen. The thermometer calibrations did not change during the three days required to obtain the data shown; the liquid helium calibration points differed by less than  $2 \times 10^{-3}$ °K, and temperatures in the range 17 to 18°K differed by no more than  $2 \times 10^{-2}$ °K, the limit of the measuring sensitivity, from day to day. The absolute uncertainty in temperature (distinct from the relative uncertainty) is of the order of  $\frac{1}{2}\%$ .

The inductance of the coil as a function of temperature was measured at 200 cps,  $H_{max} = 0.57$  oer., at 2000 cps,  $H_{max} = 3.28$  oer., and at 2000 cps,  $H_{max} = 0.10$  oer. In the course of a run, the temperature was varied at a slow enough rate ( $\lesssim .10^\circ\text{K/hr}$ ) such that the sample was in quasi-static equilibrium with the carbon resistor and the gas thermometer. The change of inductance with temperature [ $L(T) - L(4.2^\circ\text{K})$ ] is shown in Fig. 27. The curves at the right show the full transitions to the limit of the precision in temperature measurement (some inductance points have been omitted for clarity); the inset curve shows the approach of the sample to the transition to the limit of the precision in measuring the inductance of the coil. The temperatures near the horizontal arrows are the transition temperatures obtained from one half the total inductance change in the transition. The inductance change between 4.2°K and 18.2°K agrees with that calculated from the geometry of the coil and the total volume of the sample.

THIS  
PAGE  
IS  
MISSING  
IN  
ORIGINAL  
DOCUMENT

35 + 36

The present measurements are in fair agreement with previous, less accurate measurements on other  $\text{Nb}_3\text{Sn}$  coated wires. In general, it has been shown in these measurements that there is a region of rapid field penetration that is proportional to the number of wires in the sample, is independent of the thickness of the deposit, and cannot be associated with intermediate state phenomena. It is a reasonable interpretation of the present data to associate the change of inductance with temperature with a change in the penetration depth of the magnetic field in the superconducting state.

The superconducting penetration depth  $\lambda(T)$  can be shown to modify the inductance change for  $T < T_c$  in the following manner:

$$\Delta L(T) = \frac{2}{r} (\Delta L) (\lambda(T) - \lambda(0)), \quad (9)$$

where  $L(T)$  = measured inductance at temperature  $T$ ,

$$\Delta L(T) = L(T) - L(0),$$

$$\Delta L = L(> T_c) - L(0),$$

$\lambda(T)$  = penetration depth at temperature  $T$ , and

$r$  = radius of a single wire of  $2\pi r$ .

It is assumed that the inductance change is proportional to the volume of wires. It has been shown experimentally and theoretically that, to a good approximation, (Shawlow and Devlin, 1959)

$$\lambda = \lambda_0 y, \quad (10)$$

where

$$y = \left( 1 - \left( \frac{T}{T_c} \right)^4 \right)^{-1/2} \quad (11)$$

$\lambda_0$  = penetration depth at  $T = 0^\circ\text{K}$ .

From Eqs. (9) and (10) we obtain

$$\frac{d}{dy} [L(T)] = \frac{2}{r} (\Delta L) \lambda_0 \quad (12)$$

and this expression can be used unambiguously to derive  $\lambda_0$ , if  $\frac{d}{dy} [L(T)]$  can be shown to be constant.

The transition width of the present  $\text{Nb}_3\text{Sn}$  sample is  $\approx 1\%$  of  $T_c$ , approximately a factor of three larger than the percentage transition width found for such soft superconductors as tin, lead and mercury. The choice of  $T_c$  is relatively unambiguous for such materials and is usually somewhat arbitrarily chosen as the midpoint of the transition curve. (Shawlow and Devlin, 1959). In the present experiment the choice of  $T_c$  is less clear-cut and, as can be seen in Fig. 29, is somewhat critical.

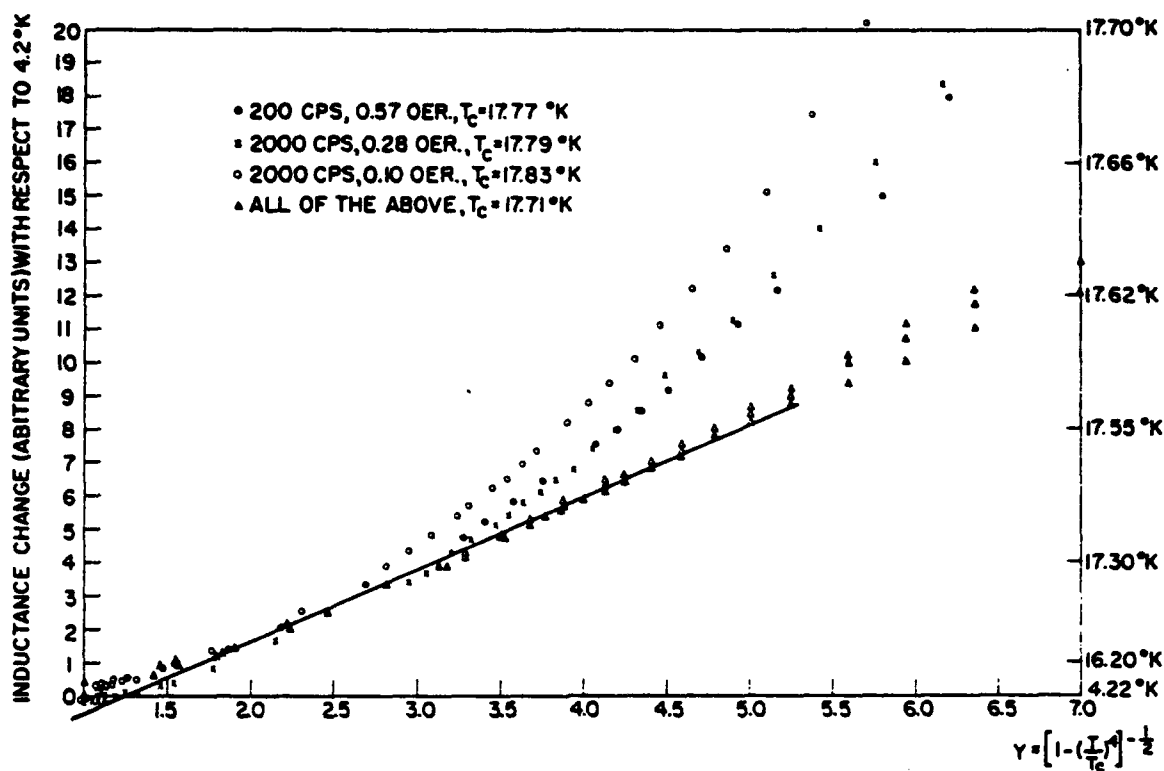


Fig. 29. Inductance change vs.  $T$  for  $\text{Nb}_3\text{Sn}$ .

Figure 29 shows the inductance changes obtained from Fig. 27 plotted against  $y$  for two sets of values of  $T_c$ . Since the inductance change can be used to construct a temperature scale for each point, this scale has been drawn on the right-hand side of the figure. The first set of points in this graph is based on values of  $T_c$  for the mid-points of the transition curve in Fig. 27. One notes that these points diverge considerably from a straight line for temperatures in excess of 17.40°K, whereas one would expect such behavior only above 17.65°K. One explanation of the discrepancy is an incorrect choice of  $T_c$ , and the second set of points shows the effect of referring all points to  $T_c = 17.71^\circ\text{K}$ . For this value all three runs follow a straight line which joins smoothly to the previous data at  $y = 3.3$  (17.4°K), and deviations occur only above  $y = 7$  (17.64°K). This functional dependence is what one would expect from Fig. 27. The value of  $\lambda_0$  obtained is 4,040 Å, which is within the uncertainty of preliminary measurements on sample 43-4 and 45-3.

The sources of random error in the determination of  $\lambda_0$  are uncertainties in temperature, the sensitivity limitation of the bridge, the choice and slope of the line  $\lambda(y) = \lambda_0 y$  and the measurement of the radius of the wires. The estimate of the error in  $\lambda_0$  due to all of these sources is less than 10%. The chief sources of systematic error which have not yet been resolved are surface roughness on a scale less than  $10^{-4}$  cm and a broader intermediate state than assumed. Photomicrographs indicate that, to the limit of resolution of optical microscopy, the perimeter could be larger than  $2\pi r$  by as much as a factor of 1.4 (Fig. 24), but electron microscopy is required to resolve this point. The final value for  $\lambda_0$  is thus 2880 Å.

Figure 30 shows the results of penetration depth measurements made on a sample of lead. One notes that for the polished state the value of  $\lambda_0$  is in good agreement with literature values of  $\lambda_0 \approx 3.9 \times 10^{-6}$  (Lock, 1951). For the etched specimen the penetration depth rose by a factor of 2.5; an effect of the same order of magnitude has been noted previously by Laurmann and Shoenberg on tin (1949).

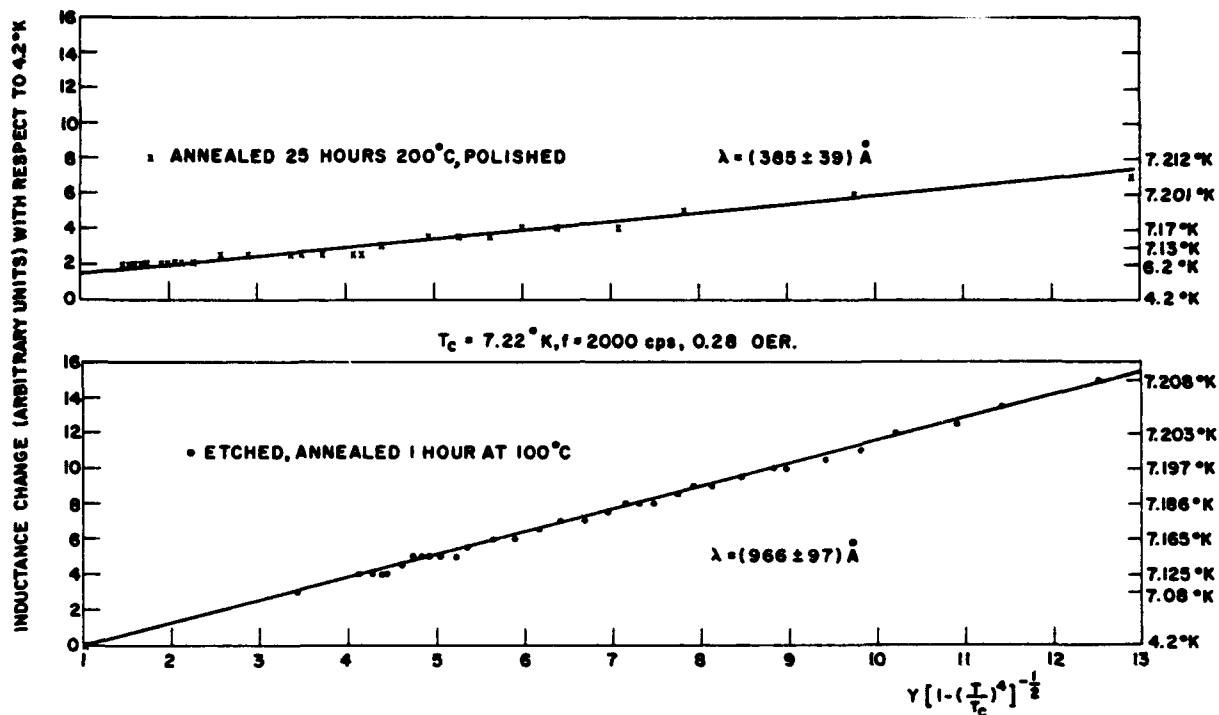


Fig. 30. Inductance change vs.  $Y$  for lead.

One can compare the present value of the penetration depth with the BCS theory on the basis of a formula originally derived by Pippard from a semiempirical treatment (Faber and Pippard, 1955):

$$\lambda_0 = \left( \frac{.18 \hbar c^2}{4 \pi (.8) \sigma k T_c} \right)^{1/2} \quad (13)$$

This expression is based on the local or London limit of the BCS theory (Miller, 1959) and has received further justification from the work of Abrikosov and Gor'kov. A review of this work is given by Goodman (1962). If one used  $T_c$  of 18°K and a resistivity of  $3 \times 10^{-5}$  ohm-cm (Cody et al, 1962) one obtains a value for  $\lambda_0$  of 1250 Å compared to the experimental value of 2880 Å. This should be considered good agreement considering possible systematic errors and theoretical uncertainties.

It is possible, however, to proceed further with a comparison of the BCS theory with  $\text{Nb}_3\text{Sn}$ . Unfortunately, the presently available data make it impossible to use anything but an effective

mass model. The four experimental parameters available are the penetration depth, the electronic specific heat (Morin and Maita, 1962), the transition temperature, and the normal state resistivity. On the basis of the local limit of the BCS theory one obtains two expressions for the Pippard coherence distance:

$$\xi_0^1 = \left( \frac{3.2\pi}{c^2} \right) \hbar (3\pi^2)^{1/3} \sigma \lambda_0^2 \frac{(\nu n_0)^{1/3}}{m^*} \quad (14)$$

and

$$\xi_0^2 = \left( \frac{.18\hbar^2}{kT_c} \right) (3\pi^2)^{1/3} \frac{(\nu n_0)^{1/3}}{m^*} \quad (15)$$

where  $\sigma$  = electrical conductivity  
 $\lambda_0$  = measured penetration depth  
 $\nu$  = number of superconducting electrons per atom  
 $n_0$  = atomic concentration  
 $m^*$  = effective mass  
 $T_c$  = transition temperature

The ratio of these two expressions is independent of  $\nu$ ,  $n_0$  and  $m^*$ , and depends only on  $\sigma$ ,  $\lambda_0$ , and  $T_c$ . Indeed one sets Eq. (14) and Eq. (15) equal to obtain Eq. (13). The discrepancy between the experimental and theoretical values of  $\lambda$  indicates the failure of consistency.

One can use the electronic specific heat ( $\gamma T$ ) to obtain  $m^* (\gamma n_0)^{1/3}$

$$\gamma T = \frac{\pi m^* k^2}{.3\hbar^2} \left( \frac{3\nu n_0}{\pi} \right)^{1/3} T \quad (16)$$

Hence, if a value of  $\gamma$  is given,  $m^*$  is determined. Given  $m^*$  one can then determine the London penetration depth  $\lambda_L$  where

$$\lambda_L = \left( \frac{m^* c^2}{4\pi\nu n_0 e^2} \right)^{1/2} \quad (17)$$

and the Fermi velocity  $v_F$  where

$$v_F = \frac{\hbar k_F}{m^*} \quad (18)$$

From the Fermi velocity and the transition temperature one can determine the Pippard coherence distance  $\xi_0$  where

$$\xi_0 = \frac{\hbar v_F}{\pi \epsilon_0} \quad (19)$$

Here  $2\epsilon_0$  is the bandgap, and from the BCS theory

$$2\epsilon_0 = 3.5 k T_c \quad (20)$$

One can then determine the mean free path  $\Lambda$  from the relation

$$\sigma = \frac{n_0 v e^2 \Lambda}{m^* v_F} \quad (21)$$

Finally, one has the BCS relation

$$\frac{H_0^2}{8\pi} = \frac{\pi m^* k^2}{3 \hbar^2} \left( \frac{3 v n_0}{\pi} \right)^{1/3} \frac{T_c^2}{4} \quad (22)$$

to determine  $H_0$ , the critical field at absolute zero (Eq. (22) is based on  $2\epsilon_0 = 3.5 k T_c$ ).

It is clear that the above-mentioned inconsistency requires a choice to be made in the value of  $\lambda_0$  or the bandgap. To obtain a consistent effective mass model it can be shown that if

$$2\epsilon_0 = A k T_c \quad (23)$$

then 
$$\lambda_0 \text{ actual} = \lambda_0 \text{ measured} \left( \frac{1}{A} \right)^{1/2} \quad (24)$$

If one assumes  $\gamma = 4.75$  to obtain a minimum effective mass (Eq. 16), and uses the following values:

$$\begin{aligned} \gamma &= 150 \times 10^{-4} \text{ cal mole deg}^{-2} \\ &= 14.1 \times 10^3 \text{ ergs/cm}^3 \text{K}^2 \text{ (Morin and Maita, 1962)} \end{aligned}$$

$$\lambda_0 = 2,880 \text{ \AA}$$

$$\sigma = 3 \times 10^{16} \text{ ohm}^{-1} \text{ cm}^{-1} \text{ (cgs) (Cody, McConville, and Rayl, 1962)}$$

$$n_0 = 5.45 \times 10^{22} \text{ atoms/cm}^3 \text{ (based on lattice constant of } 5.18 \text{ \AA)};$$

one obtains for  $2\epsilon_0 = 3.5 k T_c$  the following:

$$\lambda_0 \text{ actual} = 1250 \text{ \AA}$$

$$m^*/m = 14$$

$$\lambda_L = 390 \text{ \AA}$$

$$\Lambda = 10 \text{ \AA}$$

$$\xi_0 = 125 \text{ \AA}$$

$$v_F = 1.65 \times 10^7 \text{ cm/sec}$$

$$k_F = 1.98 \times 10^8 \text{ cm}^{-1}$$

$$H_0 = 5,000 \text{ gauss.}$$

If  $2\epsilon_0 = 1.0 kT_c$ , one obtains

$$\begin{aligned} \lambda_0 \text{ actual} &= \lambda_0 \exp = 2880 \text{ \AA} \\ m^*/m &= 14 \\ \lambda_L &= 390 \text{ \AA} \\ \Lambda &= 10 \text{ \AA} \\ \xi_0 &= 450 \text{ \AA} \\ v_F &= 1.65 \times 10^7 \text{ cm/sec} \\ k_F &= 1.98 \times 10^8 \text{ cm}^{-1} \\ H_0 &= 1,400 \text{ gauss} \end{aligned}$$

Finally, according to the theory of Wentzel (1958), Gupta and Mathur (1959), the expressions for  $\lambda_0$  and  $\xi_0$  differ by a factor of  $[NV(o)]^{1/2}$  and  $\pi$ , respectively, from the BCS formulas.  $[NV(o)]$  is the term that occurs in the BCS formula for the transition temperature

$$T_c = \langle \hbar \omega \rangle e^{-1/N(o)V} \quad (25)$$

This change does not affect the above conclusions. It is impossible to maintain the BCS value of the bandgap and the experimental values of  $\lambda_0$  on the basis of a consistent effective mass model. The required modifications are not large, however, and in view of experimental and theoretical limitations should not be considered significant. It is interesting to note, however, that there are reasons for expecting  $\lambda_0$  to be too large, since the roughness of the deposited wire is not well known. On the other hand, bandgap determinations on  $Nb_3Sn$  made in this laboratory through tunneling indicate a bandgap value approximately one half that of BCS. (Seidel and Wicklund, 1962).

Finally the above parameters permit one to calculate the parameters of the Abrikosov (1957) mixed state of hard superconductors. From Goodman (1962)

$$\kappa = \frac{.73 \lambda_L}{\Lambda} \quad (26)$$

Thus, if we choose the parameters corresponding to  $H_0 = 5,000$  gauss,  $\kappa = 28$ . This value of  $\kappa$  would predict the onset of the mixed state at  $H_{c2} = 700$  gauss, and persistence of the superconducting state to  $H_{c1} = 190,000$  gauss.

## E. LOW FIELD CRITICAL CURRENTS IN $Nb_3Sn$

Measurements were made of the quenching current as a function of magnetic field for vapor-deposited  $Nb_3Sn$  samples (Cullen, 1962). Preliminary results indicate that deposited  $Nb_3Sn$  quenches at zero field at current levels close to that predicted by the Silsbee hypothesis (Shoenberg, 1952). Furthermore, for longitudinal fields the quenching current is initially constant and then rises with the field, while in the transverse case the quenching current falls rapidly with an increasing field. As discussed in a later section, this behavior is compatible with recent theories of hard superconductors (Goodman, 1962; Parmenter, 1962) which predict that at low fields hard superconductors should behave as soft superconductors. The rise in quenching current with field can only be understood in terms of a stable domain structure that makes the current homogeneous and hence reduces the local current density.



For convenience a shunt technique was used to detect the superconducting transition. Current contacts to fairly massive copper leads were made with indium solder to nickel-plated areas at the ends of the specimen. Across the copper leads a brass shunt was soldered and potential leads placed on it. The normal resistance of the  $Nb_3Sn$  was  $60 \times 10^{-3}$  ohm (Cody, McConville and Rayl, 1962). At 4.2°K the resistance of the shunt was  $2 \times 10^{-3}$  ohm, and the total contact resistance to the specimen was  $0.2 \times 10^{-3}$  ohm. Thus, at the superconducting transition, the current through the shunt rose from 10% of the total current to 97% of the total current, and it is this change which is defined as the "quench". The total current through the sample plus shunt, and the potential drop across the shunt were monitored continuously to the quench. Separate experiments showed this technique to agree with the potential method. The maximum power dissipated at each contact was of the order of 1/3 watt, which would not appear to be excessive, since the sample was in good contact with the bath through both the substrate and the copper current leads.

Current quenching as a function of magnetic field was measured in both a 6-in. Varian magnet and a 2-in. diameter Nb-Zr solenoid. In both cases, measurements were made with the plane of the sample along the axis of the field, and rotation of the plane of the sample was made about an axis perpendicular to the axis of the field. Thus the slight amount of field distortion produced by the 40-micron specimen was the same in the rotated positions and only the angle between the current and field axis changed. As the indium current contacts were normal at 4.22°K, they did not produce any field distortion. Furthermore, the magneto-resistance of the shunt was shown to be negligible with respect to the resistance changes in the sample at the quenching current.

Preliminary results are given here for three samples, # 40-1, # 40-2 and # 40-3. In both the solenoid and the 6-in. magnet the results for samples were quantitatively similar. Sample # 40-3 was not measured in detail due to the high current level. Fig. 31 gives detailed field and rotational measurements for sample # 40-2. One notes a rise in the quenching current for longitudinal

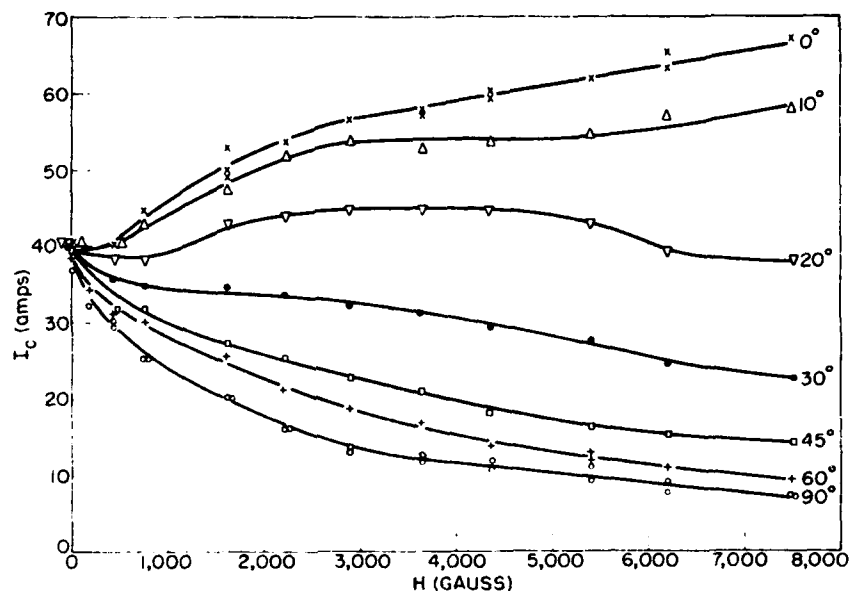


Fig. 31. Quenching current vs. field at constant angle.

fields and a rapid *fall* in the quenching current for transverse fields. The current density in transverse fields appears to flatten out around 7,000 gauss to a value that is characteristic of Nb<sub>3</sub>Sn,  $J_c \approx 10^5$  amps/cm<sup>2</sup> (Hanak, 1962). In the longitudinal case it rises to a value about 9 times this. We will first discuss the zero field transition.

Previous measurements in this laboratory (Cody, Hanak and Rayl, 1962) showed that the penetration depth of deposited Nb<sub>3</sub>Sn is about 1/2 micron; and hence, the present strip should be considered as a thick superconductor. If one assumes a Silsbee type mechanism for the zero field quench and approximates the strip by an ellipse, one obtains a quenching current  $I_c$  (Shoenberg 1952)

$$I_c = 5 a H_c$$

where  $a$  is one-half the thickness of the strip and  $H_c$  is the thermodynamic critical field. If one substitutes  $a = 21 \times 10^{-4}$  cm and  $H_c \approx 5,000$  gauss\*, one obtains  $I_c \approx 50$  amps, which is in reasonable agreement with the data of Table VI. This current would correspond to a current density  $\approx 10^8$  amps/cm<sup>2</sup>, concentrated largely at the ends of the strip.

TABLE VI  
DIMENSIONS AND FIELD DATA FOR Nb<sub>3</sub>Sn # 40

SAMPLE	WIDTH	THICKNESS	LENGTH	AREA
1	$2.40 \times 10^{-2}$ cm	$42 \times 10^{-4}$ cm	$8.8 \times 10^{-2}$ cm	$10.1 \times 10^{-5}$ cm <sup>2</sup>
2	$2.56 \times 10^{-2}$ cm	$42 \times 10^{-4}$ cm	$13.5 \times 10^{-2}$ cm	$10.8 \times 10^{-5}$ cm <sup>2</sup>
3	$6.72 \times 10^{-2}$ cm	$50 \times 10^{-4}$ cm	$34.0 \times 10^{-2}$ cm	$34.6 \times 10^{-5}$ cm <sup>2</sup>
SAMPLE	$I_c (H = 0)$	$I_c (H_{\perp} = 7500 \text{ gauss})$	$I_c (H_{\parallel} = 7500 \text{ gauss})$	
1	50 amps	14.0 amps	83 amps	
2	40 amps	7.0 amps	67 amps	
3	79 amps	32.0 amps	> 79 amps	

This is the first time for a hard superconductor that zero field quenching currents have been observed that could be interpreted by a Silsbee type mechanism. Possible reasons for the absence of observations of this mechanism in other hard superconductors are either the two-phase highly deformed nature of such materials as Nb-Zr, or the effects of contact heating at the higher zero field currents obtained for larger specimens. For example, an increase in thickness to 10 mils would increase contact heating by a factor of 25 in the present experiment and lead to contact-limited quenching.

\* See Section IV. D.

As one notes in Fig. 31, a remarkable field dependence of the quenching current is observed when the angle between the field and current is varied. This angular dependence is shown in Fig. 32 where quench currents at constant field are plotted as a function of angle. For a field longitudinal to

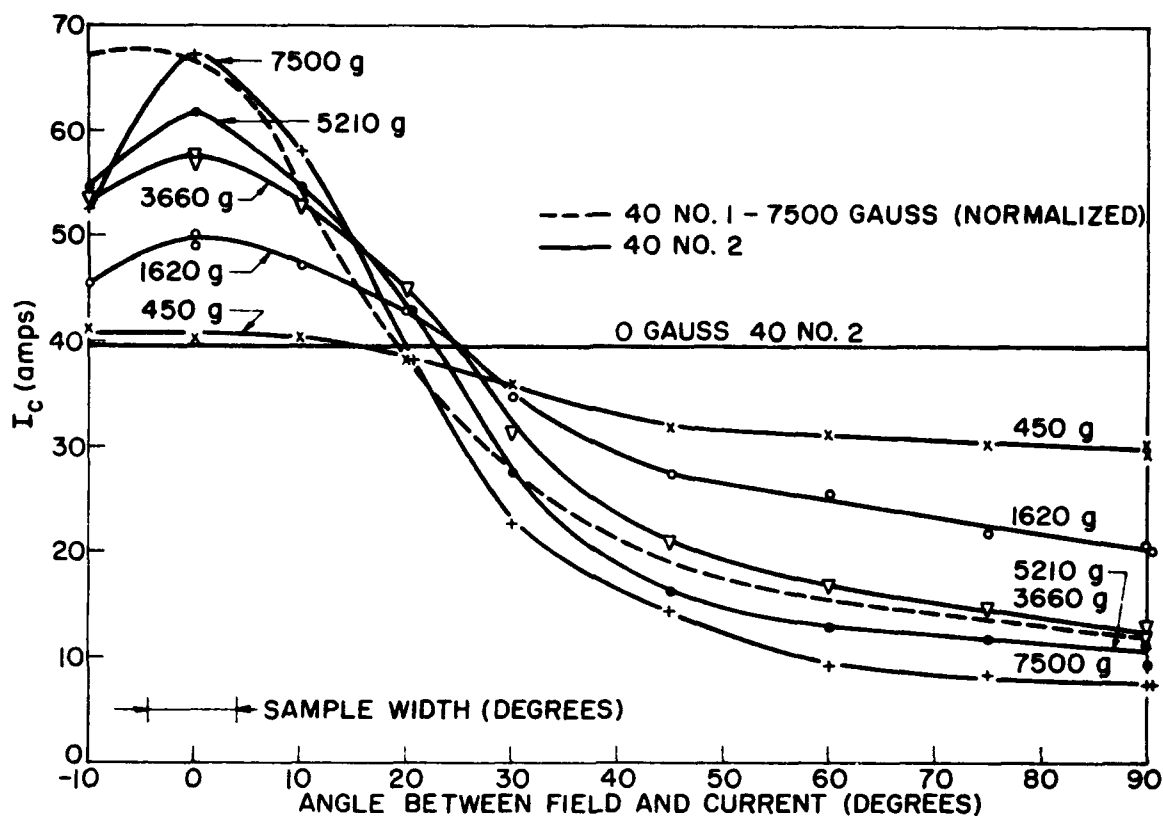


Fig. 32. Quenching current vs. angle at constant field.

the current the quenching current does not change appreciably up to  $H = 400$  gauss, and then rises rapidly to a value at 7500 gauss almost twice its zero field value. For the transverse case, on the other hand, the current decreases quite rapidly at the smallest field measured and then appears to saturate. The maximum anisotropy from longitudinal to transverse is as much as a factor of 10. Several checks were made of the reversibility of this behavior. Indeed it was possible in the longitudinal direction to destroy the superconducting state by *reducing* the field. The angular dependence shown in Fig. 32 does not follow any simple functional form. It should be emphasized that no preferred orientation is expected or found in the plane of the deposited material; and it is probable that the fall-off with angle of the current maximum can only be associated with the finite width ( $\approx 8^\circ$ ) of the specimen.

The rise in quenching current for low longitudinal fields is unexpected. It is well known at high fields that longitudinal specimens give higher quenching currents than transverse specimens

(Hart et al, 1961) but these experiments have not been continued to low fields. Figure 33 is a schematic drawing of quenching curves that are possible in terms of only the high field data. The present experiment implies that Fig. 33b is the proper curve for  $\text{Nb}_3\text{Sn}$ , and perhaps other single-phase hard superconductors. A positive slope in the quenching current as a function of field has been observed previously at medium fields, but only for cold-worked, multiphase material (Aron and Hitchcock, 1962, Hake and Leslie, 1962). In some cases it has been shown to be related to the angle between the field and the rolling direction of cold-worked material (Hake and Leslie, 1962).

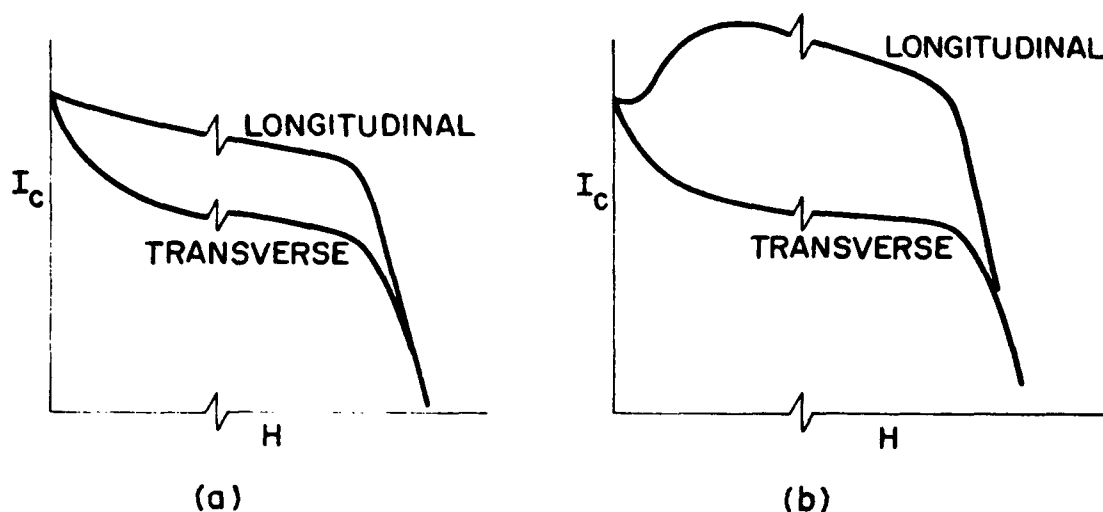


Fig. 33. Possible quenching curves (schematic).

One possible explanation of the present experiment is to be found in the theory of Ginzburg and Landau (Ginzburg and Landau, 1950, Ginzburg, 1950; Abrikosov, 1957; and Gor'kov, 1960), which has recently been reviewed by Goodman (1962) in connection with his own theoretical work on broad magnetic transitions in hard superconductors (Goodman, 1961). This theory predicts that a certain class of hard superconductors should behave identically to soft superconductors up to a field  $H_{c_2}$  less than the thermodynamic critical field  $H_c$ . At  $H_{c_2}$  these superconductors enter a mixed state, somewhat similar to the intermediate state of soft superconductors, up to a field  $H_{c_1}$ , considerably higher than  $H_c$ . These superconductors can be single-phase and dislocation free; the only requirement is that they have a penetration depth  $\lambda$  considerably greater than either the Pippard coherence distance, or the mean free path. The penetration depth measurements previously mentioned (Cody, Hanak, and Rayl, 1962) can be interpreted in terms of a semi-free-electron model\* to give the following data for  $\text{Nb}_3\text{Sn}$ :

$$\begin{aligned} \xi_0 &= \text{Pippard coherence distance} \approx 125 \text{ \AA} \\ \Lambda &= \text{mean free path} \approx 10 \text{ \AA} \\ \lambda_L &= \text{London penetration depth} \approx 390 \text{ \AA} \end{aligned}$$

\* See Section IV. D.

and one notes that the condition for the mixed state is satisfied. Indeed these values predict the following (Goodman, 1962):

$$\begin{aligned}H_{c_2} &\approx 700 \text{ gauss} \\H_c &\approx 5,000 \text{ gauss} \\H_{c_1} &\approx 190,000 \text{ gauss}\end{aligned}$$

According to this theory the material behaves as a London-type superconductor at low fields, and should quench at a current proportional to the thickness of the strip and  $H_c$ . At fields about 700 gauss, the material enters an intermediate state with domains oriented parallel to the net applied field. This state continues to fields of the order of 190,000 gauss. It is clear that this theory qualitatively fits the present preliminary data. In the mixed state for the longitudinal field the domains are parallel to the current flow, and the uniform current distribution should permit higher total currents than in the low field case where the current flow is superficial. In the transverse case the loss of symmetry leads to a domain structure perpendicular to the current flow; presumably the resultant flow path leads to regions of high local current density.

A theory due to Parmenter (1962) predicts similar behavior, but only for fields in excess of  $H_c$ . For fields less than  $H_c$  the material would behave as a soft superconductor. It is clear that this theory avoids one difficulty in explaining the present experiment in terms of the Ginzburg, Landau, Abrikosov, Gor'kov theory. Namely, it is difficult to see why  $H_c$ , and not  $H_{c_2}$  should determine the zero field quenching current. In the Parmenter (1962) theory, on the other hand,  $H_c$  arises naturally. The rise in quenching current in low longitudinal fields would follow from an intermediate state, similar to that which would arise in any soft superconductor but with unusual stability.

In summary, the present experiments indicate the existence of superficial current flow in zero field for the hard superconductor  $\text{Nb}_3\text{Sn}$  as in a soft superconductor such as tin. In transverse fields the present experiment agrees with previously examined  $\text{Nb}_3\text{Sn}$  (Hanak, 1962). In horizontal fields there is a rise in quenching current which can be interpreted as either the onset of a "mixed" or "intermediate" state which can carry higher currents than the zero field state. This is in qualitative agreement with recent theories of hard superconductors (Goodman, 1962, Parmenter, 1962). Finally it is important to note that this agreement depends on a high stability of the domain structure that is not associated with any preferred orientation or degree of cold work.

Further experimental work is necessary to ensure that the above data is representative of  $\text{Nb}_3\text{Sn}$ . The present measurements will be complemented by conventional high-sensitivity potential measurements to ensure that the quenching condition is characteristic of a superconducting-to-normal transition, and not just a low-resistance to high-resistance transition. Furthermore, if domain formation is responsible for the rise in critical currents, it will be of interest to examine the time of domain formation and decay. The temperature dependence of the quenching curves will be obtained, since it is clear that this formation will be essential for any comparison with theory.

## F. THERMAL CONDUCTIVITY OF $Nb_3Sn$

The availability of crystalline  $Nb_3Sn$  has made it possible to measure, for the first time, the thermal conductivity of this material in the interesting region below the superconducting transition. The significance of these measurements is twofold: (1) it permits the comparison of  $Nb_3Sn$  with recent theories of superconductivity (Bardeen, Rickayzen and Tewordt, 1959); and (2) through the application of a magnetic field, one can use the thermal conductivity as a probe to examine the properties of the "mixed state" of hard superconductors (Goodman, 1962; Cornish and Olsen, 1953).

In this section preliminary results are given for an unsupported, approximately 2-mil strip of deposited  $Nb_3Sn$ . For this specimen the superconductive transition starts at 16.5°K and ceases at 14.5°K. The low transition and relatively large transition width are presumably due to inhomogeneous disorder discussed in a previous section (Section IV. A.; Hanak, 1962). Since the temperature interval in the present experiment is considerably larger than the transition, it is believed that this breadth would not play an important role except in the vicinity of  $T_c$ .

The experiment will not be described in detail since the techniques are well known. A potentiometric method was used, and 1/10-watt Allen Bradley resistors calibrated with respect to a gas thermometer were used for measurement of the temperature gradient. The maximum gradient was about 1/2°K.

Figure 34 shows the temperature variation of the total thermal conductivity from 22°K to 5.5°K. Although the scale in Fig. 34 is arbitrary, the thermal conductivity at 10°K was approximately  $12 \times 10^{-3}$  watts/cm°K. One notes a linear dependence with temperature up to the start of the transition and a rapid fall-off below the transition. If one assumes the straight line dependence to be characteristic of the normal metal (i.e., dominant impurity scattering and surprisingly low lattice conductivity), one can obtain  $K_s/K_n$ , where  $K_n$  is the normal electronic conductivity and  $K_s$  is the superconducting electronic thermal conductivity. Figure 35 shows this quantity as a function of  $T/T_c$ . In Fig. 35 is also shown the theoretical temperature variation of Bardeen, Rickayzen and Tewordt (1959). The agreement between this theory and the present preliminary data on  $Nb_3Sn$  is only fair, but any interpretation requires further experimental work. It is planned to continue these measurements to lower temperature where one expects to see the onset of the phonon contribution to the thermal conductivity due to the condensation of normal electrons. Furthermore, the effect of a magnetic field will be examined, both to obtain normal state data below  $T_c$  and to obtain information on the mixed state.

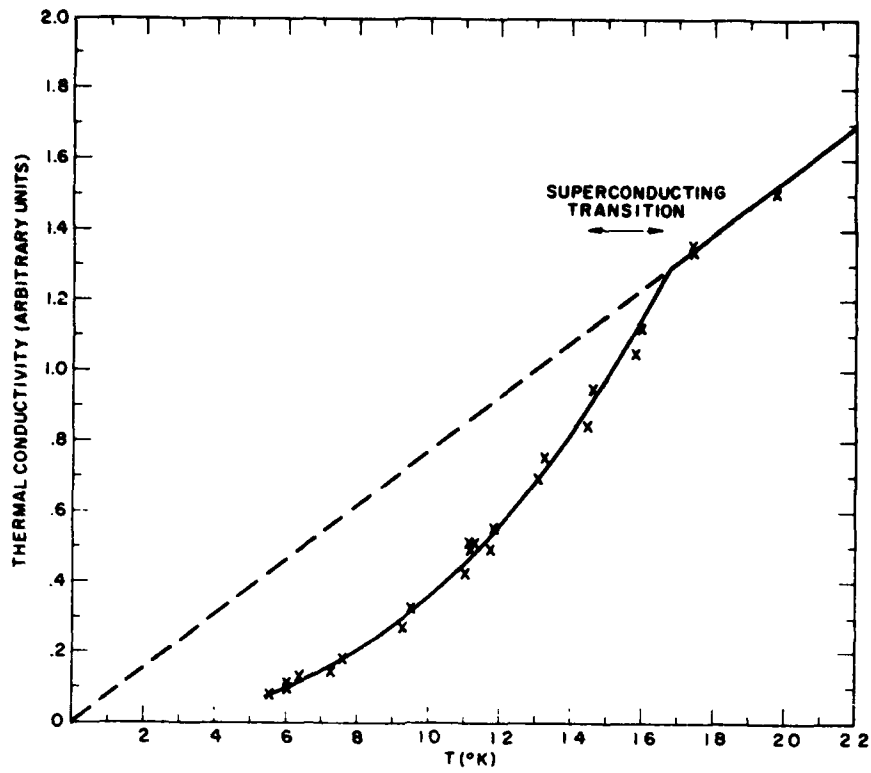


Fig. 34. Temperature variation of thermal conductivity Nb<sub>3</sub>Sn # 53.

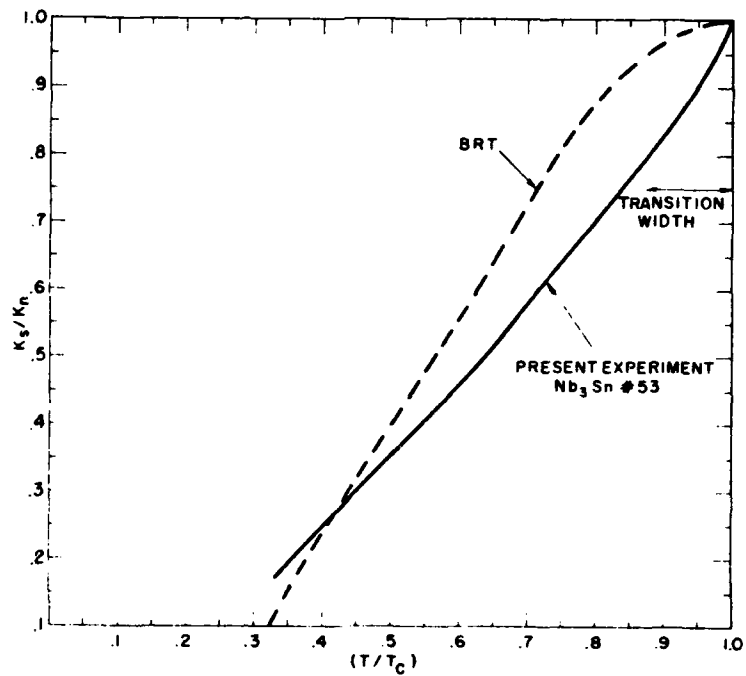


Fig. 35.  $K_s/K_n$  vs.  $T/T_c$  for Nb<sub>3</sub>Sn # 53.

## V. NEW MATERIALS

In the area of new superconductors the effort has been directed at the application of the vapor-deposition technique to other known  $\beta$ -tungsten structure compounds besides  $\text{Nb}_3\text{Sn}$ , and also to the preparation of as yet unknown  $\beta$ -tungsten structure compounds which should have high  $T_c$  on the basis of current empirical conclusions.

### A. VAPOR-DEPOSITION OF NIOBIUM GERMANIDE

The compound,  $\text{Nb}_3\text{Ge}$ , which has the  $\beta$ -tungsten structure, was first reported by Carpenter (1956), and its stability range at  $1600^\circ\text{C}$  was recently reported by the same author (1962) to be between  $\text{NbGe}_{0.159}$  ( $a = 5.177 \text{ \AA}$ ) to  $\text{NbGe}_{0.221}$  ( $a = 5.167 \text{ \AA}$ ). A specimen of  $\text{NbGe}_{0.22}$  ( $a = 5.168 \text{ \AA}$ ) was found to have a  $T_c$  of  $5.3^\circ\text{K}$  by Reed et al (1962). These materials have been prepared by a direct combination of the elements.

Vapor-phase transport of niobium germanide consisted, as previously, of chlorinating powdered mixtures of the constituent elements and reducing the resulting chlorides with hydrogen (see Fig. 1). As platinum is a convenient nucleating agent for  $\beta$ -tungsten structure compounds of niobium, in each case a piece of 0.0015 cm-thick platinum foil was placed in the deposition zone. Deposition was attempted at  $1100^\circ\text{C}$  and  $1200^\circ\text{C}$  with similar results. The deposit on the quartz walls consisted of lustrous metallic crystals of body centered tetragonal material ( $a = 10.148 \text{ \AA}$ ,  $c = 5.152 \text{ \AA}$ ) corresponding to material with composition  $\text{NbGe}_{0.54}$  reported by Nowotny et al (1956). On the platinum substrate a 0.05 cm-thick deposit of  $\beta$ -tungsten structure  $\text{Nb}_3\text{Ge}$  was formed ( $a = 5.16 \text{ \AA}$ ), which also contained traces of the tetragonal phase and a hexagonal form of  $\text{NbGe}_{0.67}$  also reported by Nowotny et al (1956). Free niobium was found deposited on quartz in a zone rich in HCl.  $T_c$  measurements were made on both the tetragonal and the  $\beta$ -tungsten specimens. The transitions were broad and near  $8^\circ\text{K}$ , which is close to that of free niobium; hence, it must be ascertained that free niobium was not present in these specimens.

### B. VAPOR-DEPOSITION OF NIOBIUM SILICIDE

In the niobium silicide system the  $\beta$ -tungsten form is not known to exist. Vapor-phase transport was attempted using the same conditions as for  $\text{Nb}_3\text{Ge}$  and also using platinum substrate for nucleation of the  $\beta$ -tungsten structure. There was no evidence of the presence of any  $\beta$ -tungsten structure material in the deposit, although lustrous crystals of at least two phases were observed. On the quartz walls the major phase consisted of a tetragonal material ( $a = 6.570 \text{ \AA}$ ,  $c = 11.884 \text{ \AA}$ ) corresponding to the compound  $\text{Nb}_5\text{Si}_3$  reported by Parthe (1955). On the platinum substrate the major phase was a tetragonal material with  $a = 10.018 \text{ \AA}$  and  $c = 5.072 \text{ \AA}$  corresponding to a high temperature form of  $\text{Nb}_5\text{Si}_3$  described by Parthe (1955). Low temperature measurements have not been made on these two materials. It is hoped to repeat the attempt at the nucleation-induced growth of  $\beta$ -tungsten structure  $\text{Nb}_3\text{Si}$  at higher temperatures.



### C. VAPOR-DEPOSITION OF VANADIUM-GALLIUM, VANADIUM SILICIDE, AND NIOBIUM-GALLIUM

The compound, vanadium-gallium ( $V_3Ga$ ), reported by Geller (1956) and formed by a direct combination of the elements, is another of a series of superconductors with the  $\beta$ -tungsten structure and a high transition temperature of 17°K. Recently it has been shown by Wernick et al (1961) that this material might remain superconducting in magnetic fields as high as 500 kilogauss. Hence, this material is extremely intriguing from the standpoint of both theory and application.

As previously, the attempted vapor-phase transport consisted of chlorinating the powdered mixture of constituent elements and reducing the chlorides with hydrogen. In these first attempts, carried out at 1100°C to 1200°C, the only product was flaky, green chloride, presumably  $VCl_2$ , which is known to be involatile at this temperature. Addition of HCl into the stream of the chlorides somewhat reduced the condensation of  $VCl_2$  perhaps by favoring the formation of the volatile chloride  $VCl_4$ . Metallic deposits consisting chiefly of elemental vanadium and gallium were obtained; it appeared that it was necessary to use high temperatures for the vapor-phase transport reactions, as well as for the volatilization of the lower valence chlorides.

As the apparatus consisted of quartz tubing and a Kanthal-wound resistance furnace, both of which were unsuitable for operation much above 1200°C, a furnace was constructed with a Crusilite (silicon carbide) heating element capable of operating up to 1400°C. Furthermore, the vapor-phase transport apparatus was made of Mullite refractory tubing capable of operating at similar temperatures.

With the aid of this apparatus attempts to prepare  $V_3Ga$  by vapor-deposition technique were continued. The problems with  $VCl_2$  condensation were solved and metallic deposits were obtained. However, they had the structure of vanadium metal. The difficulty appeared to lie in one of the following: (1) instability of  $V_3Ga$  at the temperature of the gas-phase reactions, (2) slow reduction of gallium chlorides by hydrogen, or (3) improper ratio of the metal chlorides. These possibilities were examined systematically as follows:

1. Stability experiments have been performed on arc-melted  $V_3Ga$  having initially the  $\beta$ -tungsten structure by heating the specimens in an atmosphere of helium for one hour at temperatures ranging from 950 to 1320°C, and then examining the specimens by X-ray diffraction technique. It was found that up to 1320°C the specimens retained their original structure. However, at 1320°C various products formed by a reaction of the vanadium and gallium with the Mullite container were found. It is, therefore, believed that  $V_3Ga$  is stable at these temperatures provided that an appropriate container is used.
2. Attempts to synthesize other compounds having vanadium or gallium as one of the constituents were carried out using the vapor-phase technique to determine the ease of reduction of the respective chlorides. The compound  $V_3Si$  was prepared by this method at 1320°C. However, it contained  $V_5Si_3$  as a second phase. The compound  $Nb_3Ga$  was also successfully prepared, but only after using separate chlorination tubes for the niobium and gallium. When a mixture of the two metals was used, the more reactive gallium was chlorinated first, followed by the chlorination of niobium. It is interesting that the lattice constant of the vapor-deposited  $Nb_3Ga$  ( $\beta$ -tungsten structure) was  $5.1900 \pm 0.005 \text{ \AA}$ , as compared to  $5.171 \text{ \AA}$  for the corresponding sintered material. The transition temperature of these vapor-deposited materials will be determined.
3. In view of the experience with the chlorination of the Nb, Ga mixture, future attempts to prepare  $V_3Ga$  will involve the use of separate chlorination tubes for the constituent metals.

## APPENDIX

### Thermal Effect of Resistive Current Contacts on the Quenching Current of Niobium Stannide

#### A. INTRODUCTION

In the relatively brief period of time beginning with the discovery of superconductivity of  $\text{Nb}_3\text{Sn}$  at very high magnetic fields by Kunzler et al (1961), a great deal of critical current ( $I_c$ ) vs. magnetic field ( $H$ ) data has accumulated for a variety of superconducting materials. Simultaneously with this discovery, problems were encountered with the establishment of current contacts to the superconducting specimens. In an early paper on various methods of establishing such current contacts Donadieu et al (1961) showed a large variation in the quenching current ( $I_Q$ )\* of niobium with different current contacts. Since that time workers in the field generally developed their own techniques for establishing current contacts, and they were usually satisfied when reproducible  $I_Q$  was obtained. Reproducibility is not a sufficient criterion, because it is based on the tacit assumption that the contacts are capable of delivering as much current as the specimen can carry. This is not necessarily true according to the present work.

In general, two types of current contacts can be used, superconducting and normal. In this first category the current leads to the specimen are made of a superconductor, and the contact to the specimen is established by pressure, or by a superconducting solder or weld. Such contacts can be made to carry large currents. However, they must be usually kept outside of high fields to remain superconducting.

Normal contacts, consisting of normal metal leads connected to the specimen by similar means, are not as desirable as superconducting contacts; but they are often necessary when a technique for making superconducting contacts is lacking.

With either of the two contacts it should be ascertained whether they are "adequate"; i.e., whether they enable one to measure  $I_c$  of the specimen. Perhaps the most direct way to test the contacts is to vary the contact area of the specimen until further increases in area do not cause a current increase. An experiment of this type has been performed on a  $\text{Nb}_3\text{Sn}$  vapor-deposited ribbon using normal contacts.

#### B. RESULTS AND DISCUSSION

The superconducting  $\text{Nb}_3\text{Sn}$  ribbon used consisted of a 0.0004 cm thick film deposited uniformly on the surface of a platinum ribbon substrate measuring 0.056 cm in width and 0.0046 cm in thickness. The current contacts were made by sandblasting the surface of the ribbon (to remove surface oxides), electroplating a thin layer of copper onto it, and finally soldering with soft, lead-tin solder onto copper plates measuring 1 cm  $\times$  2 cm  $\times$  1 mm and attached to a massive Teflon holder. Such contacts were always resistive because of the copper plating adjacent to the ribbon.

\*In this Appendix the critical current ( $I_c$ ) is defined as the current at which the specimen starts becoming resistive (i.e., the potential across the specimen becomes  $0.1 \mu\text{V}$ ) because of the constraints of both temperature and external magnetic field. The quenching current is defined as that current at which the specimen starts becoming resistive not only by virtue of the constraints already mentioned, but also because of added constraints imposed by "inadequate" current contacts (for example, joule heating): hence,  $I_c \geq I_Q$ .

However, at fields below 200 gauss the contact resistance was noticeably lower, because the lead-tin solder becomes superconducting. The initial length of each contact was 16 mm, and the length between the contacts was 1 cm. A brass shunt ( $R_s$ ) with a resistance of  $3.56 \times 10^{-3}$  ohms at 4.2°K was placed in parallel with the sample to protect it from damage upon current quenching and to enable one to measure the contact resistance to the specimen. The circuit diagram is shown in Fig. 36 where voltmeter  $V_1$ , with probes attached to the specimen, is used to detect superconducting to normal transition which is indicated at a voltage of  $0.1 \mu\text{V}$ . Voltmeter  $V_2$  measures

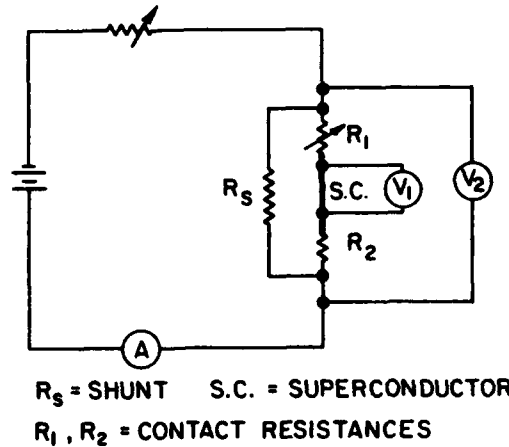


Fig. 36. Circuit diagram for quenching current measurements.

voltage  $E_2$  across the parallel circuit consisting of the shunt and the specimen including its contacts. The applied current ( $I$ ) is measured by ammeter  $A$ , the shunt current ( $I_s$ ) is determined by the relation  $I_s = \frac{E_2}{R_s}$ , and the quenching current is then obtained from  $I_Q = I - I_s$ . The sum of two contact resistances,  $R_1 + R_2 = R$ , is then simply obtained from  $R = \frac{I_s}{I_Q} R_s$ .

The experiment was performed on the same specimen by measuring  $I_Q$  at transverse dc fields of 0, 4000, and 7500 gauss, as the length of one of the contacts was varied by cutting the soldered-on ribbon in approximately 2 to 3 mm decrements from 16 mm down to 1.8 mm. The results for the quenching current vs. length (and area) of one contact are given in Fig. 37. It appears that with increasing area the quenching current tends to saturate to a constant value.

In looking for the cause of the  $I_Q$  variation, it appears safe to assume that the change in contact area per se cannot be responsible for this variation. First, such a geometric effect is unknown; and secondly, the contact area is very large with respect to the cross-sectional area of the specimen by a factor ranging from 400 to 3000. It is suggested, however, that joule heating at the contacts is responsible for this effect, because joule heating is considerable (although the contact resistance is relatively low) and it is well known that change in temperature produces a variation in  $I_c$  as pointed out by Kunzler et al (1961). Single contact resistance and the corresponding contact power dissipation,  $I_Q^2 R_1$ , were determined at the quenching current; and they appear as a function of reciprocal contact area in Fig. 38 for  $H = 0$ . The contact resistance at higher fields was only slightly higher than that shown. The deviation of the curve of contact resistance vs. reciprocal contact area from expected linearity is undoubtedly due to increasing contact resistivity with increasing power dissipation (heating) at the contacts.

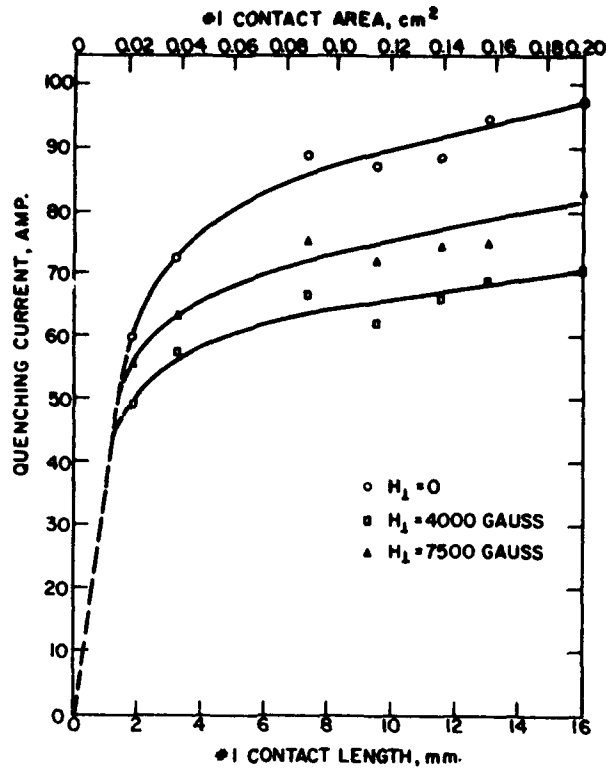


Fig. 37. Variation of quenching current with contact area.

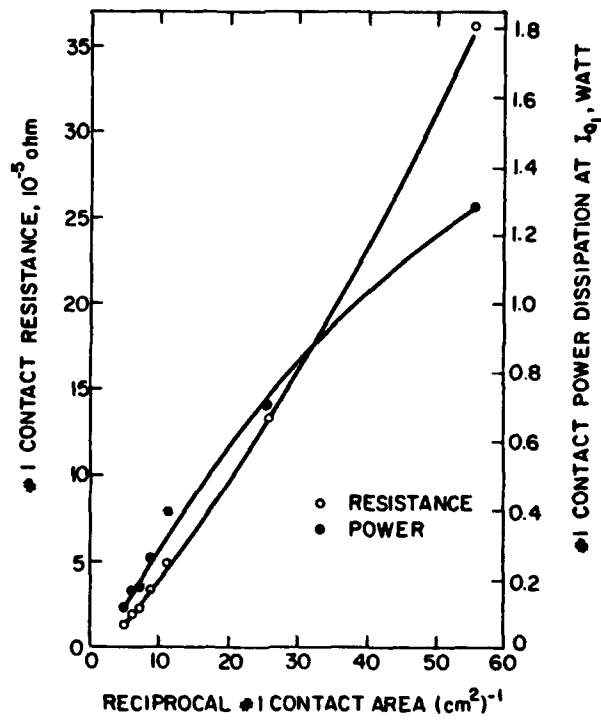


Fig. 38. Contact resistance and power dissipation vs. reciprocal contact area.

The quenching current as a function of contact power dissipation appears in Fig. 39. A nearly linear inverse variation of  $\log I_Q$  with power is observed. The extrapolation of these curves to zero power dissipation indicates a continued increase in the quenching current up to a limiting value  $I_c$ . Examination of the validity of such extrapolation is in order. If quenching

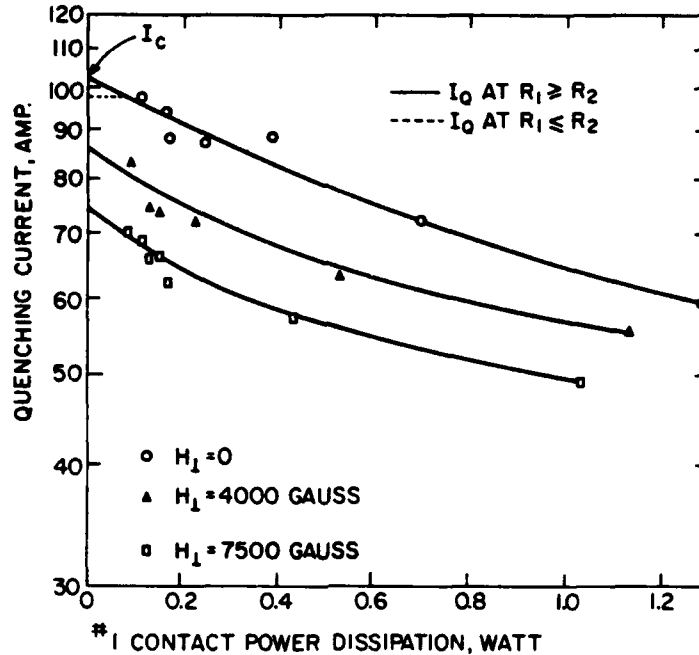


Fig. 39. Contact power dissipation vs. quenching current.

at the contacts is due to thermal effects, as supposed, then normal regions will nucleate and propagate from one or the other of the contacts, specifically from that contact which has greater  $R$  and hence  $I^2R$  loss. Thus, in the experiment described, quenching should propagate from the variable contact # 1, because its resistance,  $R_1$ , was greater than at contact # 2 (except for the first point on the left in each curve where  $R_1 = R_2$ ). If contact # 1 had been lengthened so as to make  $R_1 < R_2$ , quenching would propagate from contact # 2; and  $I_Q$  would remain constant because  $R_2$  was constant. However, at lower values of  $R_2$  and in the region  $R_1 < R_2$ , the dashed horizontal line would be displaced upward, and it would be reduced to a single point,  $I_c$ , as  $R_1$  and  $R_2$  approached zero. Thus, the extrapolation of  $I_Q$  to obtain  $I_c$  appears valid.

Experimental proof of the occurrence of the horizontal region (and hence of changing of the quenching site) was obtained in a manner similar to the above experiment, except that the starting contacts were made of unequal length such that  $R_1 < R_2$ . The results are shown in Fig. 40, where in the range,  $R_1 < R_2$  to  $R_1 = R_2$ , the quenching current is constant indicating that quenching propagates from contact # 2. In the range  $R_1 = R_2$  to  $R_1 > R_2$ , the quenching current decreases indicating quenching at contact # 1.

Figure 39 can be used to estimate the rate of variation of  $I_Q$  with power dissipation by determining the average slope of  $I_Q$ . Data in Fig. 39 have the form

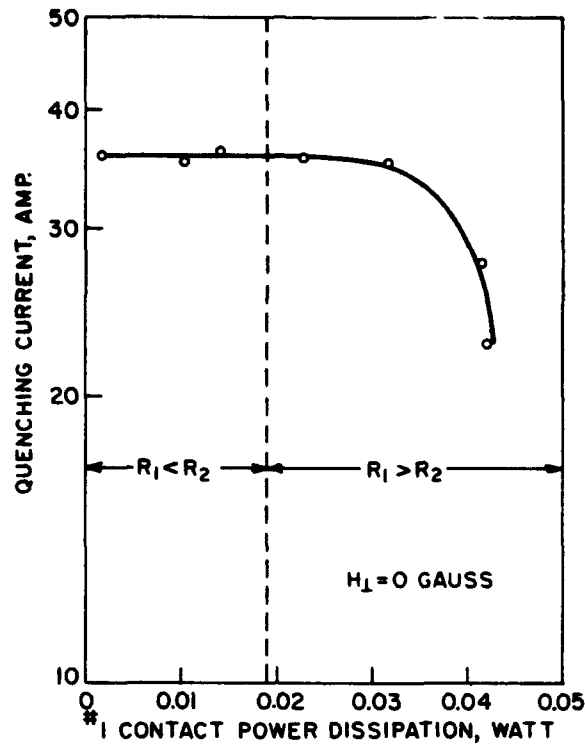


Fig. 40. Contact power dissipation vs. quenching current.

$$\log I_{Q1} = f(P) + c \quad (27)$$

which have the slope

$$\frac{1}{I_{Q1}} \frac{dI}{dP} = f'(P) \approx m(P) \quad (28)$$

Here  $m(P)$  represents the power coefficient of current variation. At  $H = 0$  the average value of  $m(P)$  is  $-0.44$  per watt, meaning that the quenching current decreases at a rate of 44 percent per watt.

As mentioned above,  $I_c$  is known to vary inversely with bath temperature. The temperature coefficient of quenching current variation,

$$\frac{1}{I_Q} \frac{dI}{d(T_c - T)} = n(T_c - T), \quad (29)$$

for "cored"  $Nb_3Sn$  wire was estimated to have a nearly constant value of  $0.22 (^\circ K)^{-1}$  over a wide range of magnetic field (20 to 88 kilogauss) from data on  $I_c$  vs.  $H$  at  $4.2^\circ K$  and  $1.5^\circ K$ , reported by Kunzler et al (1961). As joule heating at the contacts is tantamount to bath temperature variation, so far as the specimen is concerned, the power and temperature coefficients of

quenching current variation (Eqs. 28 and 29) are simply related in terms of temperature dependence on power dissipation. This dependence can be obtained from the ratio of the respective coefficients; namely,

$$\frac{m(P)}{n(T_c - T)} = \frac{-0.44}{0.22} = 2^\circ\text{K/watt}, \quad (30)$$

indicating that the temperature rise at the contacts in the present experiment was 2°K per watt of dissipated power.

From the data presented, it is evident that when normal contacts are used the quenching current,  $I_Q$ , is always smaller than the critical current,  $I_c$ . When such contacts are used, it is therefore imperative to determine the contact resistance, contact power dissipation and the dependence of the quenching current on power, to make appropriate corrections for the contact power dissipation. Otherwise, any correlation involving the "critical current" is not definitive. For example, the apparent variation of the  $J_c$  of Nb-Zr wire with diameter, observed by Betterton et al (1962), should be re-examined in view of these results.

Use of superconducting contacts should enable one to measure  $I_c$  directly without the need for correction for contacts. However, even here the contacts must carry at least as much current as the specimen. Analogous contact area analysis can be used.

## REFERENCES

- Abrikosov, A. A., (1957), *Soviet Phys. - JETP* **5**, 1174.
- Aron, P. R. and Hitchcock, H. C., (1962 a), Lawrence Radiation Laboratory, Berkeley, California - Private Communications.
- Aron, P. R. and Hitchcock, H. C., (1962 b), University of California, Lawrence Radiation Laboratory Report UCRL-10087.
- Bardeen, J., Cooper, L. N., and Schrieffer, J.R., (1957), *Phys. Rev.* **108** 1175.
- Bardeen, J., Rickayzen, G., and Tewordt, L., (1959), *Phys. Rev.* **113**, 982.
- Betterton, J. O., Kneip, J. D., Jr., Easton, D. S., and Scarborough, J. O., (1962), *J. Metals* **14**, 74.
- Bleaney and Bleaney, (1957), *Electricity and Magnetism* (Oxford University Press) p. 438.
- Carpenter, J. H., (1956), Thesis, Purdue University
- Carpenter, J. H., (1962), *J. Phys. Chem.* (In Press).
- Challis, L. J., (1960), Proc. VII Int. Conf. on Low Temp. Phys., Toronto, University of Toronto Press, p. 476.
- Cherry, W. H. and Gittleman, J. I., (1960), paper given at Symposium on Superconducting Techniques for Computing Systems, Washington D. C., May 17-19, 1960.
- Cody, G. D., Hanak, J. and Rayl, M., (1962), Proc. VIII Int. Conf. on Low Temp. Phys., London, Sept. 16-23, (to be published).
- Cody, G. D., Mc Conville, G. T., and Rayl M., (1962), RCA Laboratories, (to be published).
- Cornish, F. H. J. and Olsen, J.L., (1953), *Helv. Phys. Acta* **26**, 369.
- Cullen, G., (1962) RCA Laboratories, (to be published).
- Donadiou, L. J., (1961), Conference on Fundamental Research in Superconductivity, IBM, Yorktown, N.Y., June 16-18 (unpublished).
- Faber, T. E. and Pippard, A. B., (1955), *Proc. Roy. Soc.* **A231**, 336.
- Geller, S., (1956), *Acta. Cryst.* **9**, 885.
- Giaver, I. and Megerle, K., (1961), *Phys. Rev.* **122**, 1101.
- Ginzburg, V. L., (1950), *Nuovo Cimenti* **2**, 1234.
- Ginzburg, V. L. and Landau, L. D., (1950), *J. Exptl. and Theor. Phys. (USSR)* **20**, 1064.
- Gonser, B. W. and Slowter, E. E., (1938), "The coating of Metals with Tin from the Vapor Phase," Tech. Publ. International Tin Research and Development Council, New York.
- Goodman, B. B., (1961), *Phys. Rev. Letters* **6**, 597.
- Goodman, B. B., (1962), *IBM J. Research and Development* **6**, 63.
- Gor'kov, L. P., (1960), *Sov. Phys. JETP* **10**, 998.
- Gupta, K. K., and Mathur, U.S., (1959) *Phys. Rev.* **115**, 75.
- Hake, R. R. and Leslie, D. H., (1962), Proc. VIII Int. Conf. on Low Temp. Phys., London, Sept. 16-23, (to be published).
- Hanak, J. J., (1962), Proc. Conf. on Advanced Electronic Materials, Met. Society AIME, Philadelphia, Aug. 27-29, (to be published).



- Hanak, J. J., Cody, G. D., Aron, P. R. and Hitchcock, H. C., (1961), Proc. Int. Conf. on High Mag. Fields, MIT Press, p. 592.
- Hanak, J. J., Cody, G. D., Cooper, J. L. and Rayl, M., (1962), Proc. VIII Int. Low Temp. Phys. Conf., London, Sept 16-23, (to be published).
- Hart, Jacobs, Kolbe, and Lawrence, (1961), Proc. Int. Conf. on High Mag. Fields, MIT Press, p. 584.
- Hulm, J. K., (1962), Bull. Amer. Phys. Soc. II, 7, 197.
- Jansen, H. G. and Saur, E. J., (1960), Proc. VII Int. Conf. Low Temp. Phys., Toronto, University of Toronto Press, p. 379.
- Kapitza, P. L., (1941), J. Exptl. Theoret. Phys. (USSR) 11, 1.
- Khalatnikov, I. M., (1952), J. Exptl. Theoret. Phys. (USSR) 22, 687.
- Kunzler, J. E., Buehler, E., Hsu, F. J. L., and Wernick, J. H., (1961), Phys. Rev. Letters 6, 89.
- Kunzler, J. E., (1961), Proc. of Int. Conf. on High Mag. Fields, MIT Press, p. 574.
- Laurmann, E. and Shoenberg, D., (1949), Proc. Roy. Soc. A198, 560.
- Lindenfeld, P., (1961), Private Communication.
- Little, W. A., (1959), Can. J. Phys. 37, 334.
- Little, W. A., (1961), Phys. Rev. 123, 435.
- Lock, J. M., (1951). Proc. Roy. Soc. A208, 391.
- Lynton, E. A., (1962), *Superconductivity*, Methuen, London, p. 80.
- Meissner, R. H., (1960), Phys. Rev. 117, 672.
- Miller, P. B., (1959), Phys. Rev. 113, 1209.
- Morin, L. P., and Maita, J. P., (1962), Bell Telephone Laboratories, (to be published).
- Nevitt, M. V., (1958), Trans. AIME, 212, 319.
- Nowotny, H., Searcy, A. W., and Orr, J. E., (1956), J. Phys. Chem. 60, 677.
- Parmenter, R. H., (1960), Phys. Rev. 118, 1173.
- Parmenter, R. H., (1962), RCA Review 23, 323.
- Parthe, (1955), Monatsh. Chem. 86, 385.
- RCA, (1961), "Superconductivity in Metals and Alloys-Technical Documentary Report No. ASD-TDR-62-269, Contract No. AF 33(616)-6405.
- Reed, T. B., Gatos, H. C., LaFleur, W. J. and Roddy, J. T., (1962), Proc. Conf. on Advanced Electronic Materials, Met. Society AIME, Phil. August 27-29, (to be published).
- Salter, L. C., Jr., Autler, S. H., Kolm, H. H., Rose, D. J., and K. Goen, (1961). Proc. Int. Conf. on High Mag. Fields, MIT Press, p. 344.
- Seidel, T., and Wicklund, A. W., (1962), Proc VIII Int. Low Temp. Phys. Conf., London, Sept. 16-23 (to be published).
- Shapiro, Smith, Miles and Nicol, (1961), Phys. Rev. Letters 6, 686.
- Shawlow, A. L., and Devlin, G. E., (1959), Phys. Rev. 113, 120.

- Sherrill, M. D. and Edwards, H. H., (1961), *Phys. Rev. Letters* **6**, 460.
- Shiffman, C., (1961), *Annual Report 1961-1962 M.I.T. - Materials Service and Engineering*.
- Shoenberg, D., (1952), *Superconductivity*, Cambridge University Press, p. 150.
- Sibert, M. E., Kolk, A. J., Jr., and Steinberg, M. A., (1958), *Technology of Columbium, (Niobium)*, ed B. Gonser and E. M. Sherwood, Electrochem Soc., Wiley, New York; Chapman and Hill, London.
- Wenzel, G., (1958), *Phys. Rev.* **111**, 1488.
- Wernick, J. H., Morin, F. J., Hsu, F. S. L., Dorsi, D. Maita, J. P., and Kunzler, J. E., (1961), *Proc. Int. Conf. on High Mag. Fields*, MIT Press, p. 609.
- Wyman, L. L., Cuthill, J. R., Moore, G. A., Park, J. J., and Yakowitz, H. (1962), *J. Research Nat. Bur. Standards* **66A**, 351.
- Zimmerman, J. E., (1961), *Rev. Sci. Inst.* **32**, 402.

<p>Aeronautical Systems Division, Dir./Materials &amp; Processes Physics Lab. Wright Patterson AFB, Ohio. Rpt. No. ASD-TDR-62-1111. SUPERCONDUCTIVITY IN METALS AND ALLOYS. Final Rpt., Feb. '63, 70 p., incl. illus., tables, 65 refs.</p> <p style="text-align: center;">Unclassified Report</p> <p>Measurements were made of the Kapitza resistance in tin, indium and sapphire and its change at the superconducting transition. An attempt to detect an electric field dependence of the Kapitza resistance in platinum had negative results.</p> <p>A new method for the preparation of <math>\beta</math>-tungsten compound superconductors, such as Nb<sub>3</sub>Sn, was developed. Properties of the deposited material and the extension of this method to such possible <math>\beta</math>-tungsten compounds as niobium germanide, niobium silicide, vanadium-gallium, vanadium silicide and niobium-gallium are described.</p> <p>The transition temperature of niobium stannide is shown to depend not only on the stoichiometry, but also on the state of order of the lattice. Resistivity of Nb<sub>3</sub>Sn is given as a function of temperature from 4.2°K to 370°K. Tunneling measurements on deposited Nb<sub>3</sub>Sn indicate the existence of a <span style="border: 1px solid black; border-radius: 50%; padding: 2px;"> </span> (over)</p>	<p>1. Superconductors 2. Niobium Stannide</p> <p>I. AFSC Proj 7371, Task 737102</p> <p>II. Contract No. AF33(657)-7733</p> <p>III. RCA Laboratories, Princeton, N. J.</p> <p>IV. Cherry, W. H., Cody, G. D., et al.</p> <p>V. Aval fr OTS</p> <p>VI. In ASTIA collection</p>	<p>Aeronautical Systems Division, Dir./Materials &amp; Processes Physics Lab. Wright Patterson AFB, Ohio. Rpt. No. ASD-TDR-62-1111. SUPERCONDUCTIVITY IN METALS AND ALLOYS. Final Rpt., Feb. '63, 70 p., incl. illus., tables, 65 refs.</p> <p style="text-align: center;">Unclassified Report</p> <p>Measurements were made of the Kapitza resistance in tin, indium and sapphire and its change at the superconducting transition. An attempt to detect an electric field dependence of the Kapitza resistance in platinum had negative results.</p> <p>A new method for the preparation of <math>\beta</math>-tungsten compound superconductors, such as Nb<sub>3</sub>Sn, was developed. Properties of the deposited material and the extension of this method to such possible <math>\beta</math>-tungsten compounds as niobium germanide, niobium silicide, vanadium-gallium, vanadium silicide and niobium-gallium are described.</p> <p>The transition temperature of niobium stannide is shown to depend not only on the stoichiometry, but also on the state of order of the lattice. Resistivity of Nb<sub>3</sub>Sn is given as a function of temperature from 4.2°K to 370°K. Tunneling measurements on deposited Nb<sub>3</sub>Sn indicate the existence of a <span style="border: 1px solid black; border-radius: 50%; padding: 2px;"> </span> (over)</p>	<p>1. Superconductors 2. Niobium Stannide</p> <p>I. AFSC Proj 7371, Task 737102</p> <p>II. Contract No. AF33(657)-7733</p> <p>III. RCA Laboratories, Princeton, N. J.</p> <p>IV. Cherry, W. H., Cody, G. D., et al.</p> <p>V. Aval fr OTS</p> <p>VI. In ASTIA collection</p>
<p>Aeronautical Systems Division, Dir./Materials &amp; Processes Physics Lab. Wright Patterson AFB, Ohio. Rpt. No. ASD-TDR-62-1111. SUPERCONDUCTIVITY IN METALS AND ALLOYS. Final Rpt., Feb. '63, 70 p., incl. illus., tables, 65 refs.</p> <p style="text-align: center;">Unclassified Report</p> <p>Measurements were made of the Kapitza resistance in tin, indium, and sapphire and its change at the superconducting transition. An attempt to detect an electric field dependence of the Kapitza resistance in platinum had negative results.</p> <p>A new method for the preparation of <math>\beta</math>-tungsten compound superconductors, such as Nb<sub>3</sub>Sn, was developed. Properties of the deposited material and the extension of this method to such possible <math>\beta</math>-tungsten compounds as niobium germanide, niobium silicide, vanadium-gallium, vanadium silicide and niobium-gallium are described.</p> <p>The transition temperature of niobium stannide is shown to depend not only on the stoichiometry, but also on the state of order of the lattice. Resistivity of Nb<sub>3</sub>Sn is given as a function of temperature from 4.2°K to 370°K. Tunneling measurements on deposited Nb<sub>3</sub>Sn indicate the existence of a <span style="border: 1px solid black; border-radius: 50%; padding: 2px;"> </span> (over)</p>	<p>1. Superconductors 2. Niobium Stannide</p> <p>I. AFSC Proj 7371, Task 737102</p> <p>II. Contract No. AF33(657)-7733</p> <p>III. RCA Laboratories, Princeton, N. J.</p> <p>IV. Cherry, W. H., Cody, G. D., et al.</p> <p>V. Aval fr OTS</p> <p>VI. In ASTIA collection</p>	<p>Aeronautical Systems Division, Dir./Materials &amp; Processes Physics Lab. Wright Patterson AFB, Ohio. Rpt. No. ASD-TDR-62-1111. SUPERCONDUCTIVITY IN METALS AND ALLOYS. Final Rpt., Feb. '63, 70 p., incl. illus., tables, 65 refs.</p> <p style="text-align: center;">Unclassified Report</p> <p>Measurements were made of the Kapitza resistance in tin, indium and sapphire and its change at the superconducting transition. An attempt to detect an electric field dependence of the Kapitza resistance in platinum had negative results.</p> <p>A new method for the preparation of <math>\beta</math>-tungsten compound superconductors, such as Nb<sub>3</sub>Sn, was developed. Properties of the deposited material and the extension of this method to such possible <math>\beta</math>-tungsten compounds as niobium germanide, niobium silicide, vanadium-gallium, vanadium silicide and niobium-gallium are described.</p> <p>The transition temperature of niobium stannide is shown to depend not only on the stoichiometry, but also on the state of order of the lattice. Resistivity of Nb<sub>3</sub>Sn is given as a function of temperature from 4.2°K to 370°K. Tunneling measurements on deposited Nb<sub>3</sub>Sn indicate the existence of a <span style="border: 1px solid black; border-radius: 50%; padding: 2px;"> </span> (over)</p>	<p>1. Superconductors 2. Niobium Stannide</p> <p>I. AFSC Proj 7371, Task 737102</p> <p>II. Contract No. AF33(657)-7733</p> <p>III. RCA Laboratories, Princeton, N. J.</p> <p>IV. Cherry, W. H., Cody, G. D., et al.</p> <p>V. Aval fr OTS</p> <p>VI. In ASTIA collection</p>

<p>bandgap (<math>2\epsilon_0</math>). Preliminary results are compatible with the relation: <math>2\epsilon_0 \approx 1.8 T_C</math>. Thermal conductivity measurements were made on Nb<sub>3</sub>Sn from 4.2°K to 25°K.</p> <p>Penetration depth measurements were made on deposited Nb<sub>3</sub>Sn. The temperature dependence is similar to that obtained for other superconductors, but the value of the penetration depth at <math>T = 0^\circ\text{K}</math> (2,880 Å) is almost an order of magnitude larger than that observed for soft superconductors.</p> <p>Quenching currents were measured on deposited Nb<sub>3</sub>Sn. For transverse fields the quenching current drops rapidly, whereas for longitudinal fields the quenching current rises.</p>		<p>bandgap (<math>2\epsilon_0</math>). Preliminary results are compatible with the relation: <math>2\epsilon_0 \approx 1.8 T_C</math>. Thermal conductivity measurements were made on Nb<sub>3</sub>Sn from 4.2°K to 25°K.</p> <p>Penetration depth measurements were made on deposited Nb<sub>3</sub>Sn. The temperature dependence is similar to that obtained for other superconductors, but the value of the penetration depth at <math>T = 0^\circ\text{K}</math> (2,880 Å) is almost an order of magnitude larger than that observed for soft superconductors.</p> <p>Quenching currents were measured on deposited Nb<sub>3</sub>Sn. For transverse fields the quenching current drops rapidly, whereas for longitudinal fields the quenching current rises.</p>	
<p>bandgap (<math>2\epsilon_0</math>). Preliminary results are compatible with the relation: <math>2\epsilon_0 \approx 1.8 T_C</math>. Thermal conductivity measurements were made on Nb<sub>3</sub>Sn from 4.2°K to 25°K.</p> <p>Penetration depth measurements were made on deposited Nb<sub>3</sub>Sn. The temperature dependence is similar to that obtained for other superconductors, but the value of the penetration depth at <math>T = 0^\circ\text{K}</math> (2,880 Å) is almost an order of magnitude larger than that observed for soft superconductors.</p> <p>Quenching currents were measured on deposited Nb<sub>3</sub>Sn. For transverse fields the quenching current drops rapidly, whereas for longitudinal fields the quenching current rises.</p>		<p>bandgap (<math>2\epsilon_0</math>). Preliminary results are compatible with the relation: <math>2\epsilon_0 \approx 1.8 T_C</math>. Thermal conductivity measurements were made on Nb<sub>3</sub>Sn from 4.2°K to 25°K.</p> <p>Penetration depth measurements were made on deposited Nb<sub>3</sub>Sn. The temperature dependence is similar to that obtained for other superconductors, but the value of the penetration depth at <math>T = 0^\circ\text{K}</math> (2,880 Å) is almost an order of magnitude larger than that observed for soft superconductors.</p> <p>Quenching currents were measured on deposited Nb<sub>3</sub>Sn. For transverse fields the quenching current drops rapidly, whereas for longitudinal fields the quenching current rises.</p>	